NUMERICAL MODELING OF WATER WAVE PROPAGATION USING THE MESHLESS MULTIQUADRIC METHOD

by

Yavuz Tokmak

B.S.,Civil Engineering, Boğaziçi University,2002

Submitted to the Institute for Graduate Studies in
Science and Engineering in partial fulfillment of
the requirements for the degree of
Master of Science

Graduate Program in Civil Engineering
Boğaziçi University
2005

NUMERICAL MODELING OF WATER WAVE PROPAGATION USING THE MESHLESS MULTIQUADRIC METHOD

APPROVED BY:

Assoc. Prof. Osman S. Börekçi (Thesis Supervisor)	.....
Prof. Dr. Cem Avcı	.....
Asst. Prof. Yasin Fahjan	.....
Assoc. Prof. Emre N. Otay	.....
Assoc. Prof. Haluk Örs	.....

DATE OF APPROVAL: 15.09.2005

ACKNOWLEDGEMENTS

I would like express my deep and sincere gratitude to my supervisor Dr. Osman Börekçi for his guidance which have provided a good basis for this thesis. Gratitude also goes to my friends Bilge Alıcıoğlu, Esra Mete Güneyisi, Cenk Güngör for their friendship that I definitely needed at the critical moments.

Finally, I am very grateful to my grandmother Nevriye, my mother Hatice and my uncle Mesut Güçlü for their love, patience and support. This work is dedicated to my grandfather Ali Güçlü whom I have missed too much since the day he passed away in 1988.

ABSTRACT

NUMERICAL MODELING OF WATER WAVE PROPAGATION USING THE MESHLESS MULTIQUADRIC METHOD

In the present study, water wave propagation in two dimensions, where the flow is irrotational, is numerically modeled using meshless multiquadric (MQ) method. In the first part, the method is applied to the classical linear wave theory boundary value problem. In the second part, the linear problem is modified to investigate how the solutions are affected under fully nonlinear free surface boundary conditions where the free surface deformation needs to be dealt with. The model that is developed in the third part, uses the fully nonlinear free surface boundary conditions and accepts nonlinear stream function wave input. The results of the numerical tests show that the linear waves and nonlinear waves are predicted with excellent accuracy with meshless MQ method.

ÖZET

DOĞRUSAL VE DOĞRUSAL OLMAYAN SU DALGASI İLERLEMESİNİN AĞSIZ MQ YÖNTEMİ İLE SAYISAL MODELLENMESİ

Bu çalışmada akışın çevrintisiz olduğu iki boyutta su dalgası ilerlemesi ağsız MQ yöntemi ile sayısal olarak modellenmiştir. İlk bölümde, yöntem klasik doğrusal dalga teorisi sınır değeri problemine uygulanmıştır. İkinci bölümde doğrusal problem, yüzey değişiminin hesaba katılmasının gerektiği doğrusal olmayan serbest yüzey sınır şartları altında çözümlerin nasıl etkilendiğini araştırmak için değiştirilmiştir. Üçüncü bölümde geliştirilen model doğrusal olmayan serbest yüzey sınır şartlarını kullanmakta ve doğrusal olmayan akış fonksiyonlarını girdi olarak kabul etmektedir. Sayısal deneylerin sonuçları ağsız MQ yöntemi ile doğrusal ve doğrusal olmayan dalgaların mükemmel doğrulukta tahmin edilebildiğini göstermiştir.

TABLE OF CONTENTS

LIST OF FIGURES

LIST OF TABLES

LIST OF SYMBOLS/ABBREVIATIONS

a	Wave amplitude
$\mathbf{A}$	Coefficient matrix of a linear system
A_{ij}	Entry of coefficient matrix $\mathbf{A}$ at the ith row, jth column
A_{ij}^{-1}	Entry of coefficient matrix $\mathbf{A}$'s inverse at the ith row, jth column
$\mathbf{b}$	Right hand side vector of a linear system
B_0	Partial differential boundary operator
c	Radial basis function shape parameter
C	Wave phase speed
C_0	Linear wave phase speed
$C'(t)$	Time dependent Bernoulli constant
f	Right hand side of a field equation
f_b	Function of the bottom surface
f_d	First order derivative of a function
g	Gravitational acceleration
g_o	Right hand side of a boundary equation
h	Depth
H	Wave height
k	Wave number
k_i^{Ξ}	ith derivative of dependent parameter Ξ in 4th order Runge-Kutta method
L	Wave length
L_0	Partial differential field operator
M	Number of additional centers outside the domain
M_a	Order of augmentation
N	Number of collocation or data centers
n_o	Order of accuracy in Higdon radiation boundary condition
$\mathbf{n}$	Unit normal vector

N'	Number of collocation centers both on the boundary and internal region
N_s	Order of stream function
p	Pressure at the surface
$\mathbf{P}$	Coefficient matrix corresponding to the augmented polynomials
P_{ij}	Entry of coefficient matrix corresponding to the augmented polynomials at the ith row, jth column
p_k	Polynomials used in augmentation
$\mathbf{P^T}$	Transpose of $\mathbf{P}$
p'	A compactly supported univariate polynomial
r	Distance between two collocation centers
r'	Radial distance
s	Interpolant
t	Time
T	Wave period
t_0	Time at the beginning of a surface particle's motion
u	Horizontal component of velocity in the direction of flow
$\mathbf{u}$	Velocity vector
u_b	Normal velocity of the bottom boundary
u_i	Horizontal velocity component at the center i
u_L	Lagrangian particle velocity in the direction of flow
u_s	Normal velocity component of seepage through the bottom boundary
$\overline{u}$	Mean fluid speed relative to the wave
v	Vertical component of velocity
w	Horizontal component of velocity transverse to the direction of flow in the Cartesian System
W	Width of the solution domain
w_L	Lagrangian particle velocity in the vertical
x	Horizontal coordinate component in the direction of flow
x_0	Horizontal component of the velocity of the initial position of a surface particle

x_f	Horizontal Cartesian component of a fixed point
x_L^f	Horizontal Lagrangian component of a fixed point
z_L^f	Vertical Lagrangian component of a fixed point
x_f	Horizontal Cartesian component of a fixed point
x_L	Horizontal component of a particle's position in Lagrangian view
y	Horizontal coordinate component transverse to the direction of flow in the Cartesian System
$\mathbf{y}$	Data values vector
z	Vertical coordinate component in the Cartesian System
z_0	Vertical component of the velocity of the initial position of a surface particle
z_L	Vertical component of a particle's position in Lagrangian view
$\boldsymbol{\alpha}$	Vector of interpolation coefficients
α_i	ith interpolation coefficient
$\boldsymbol{\alpha}^{\boldsymbol{T}}$	Transpose of $\boldsymbol{\alpha}$
β_k	kth coefficient of augmented polynomials
Δt	Time step
ϕ	Velocity potential
$\mathbf{\Phi}$	Coefficient matrix of interpolation
ϕ_i	Velocity potential at the center i
Φ_{ij}	Entry of interpolation matrix at the ith row, jth column
ϕ_L	Lagrangian velocity potential
ϕ_s	Velocity potential at the surface
φ	Radial basis function
η	Free surface displacement
θ_n	Angle between the boundary normal and direction of outgoing waves
ρ	Density of water
ω	Wave angular frequency
Ω	Problem domain

$\partial\Omega$	Problem boundary
$\partial\Omega_s$	Free surface boundary
$\partial\Omega_b$	Bottom boundary
$\partial\Omega_i$	Influx boundary
$\partial\Omega_r$	Radiation boundary

CFL	Courant-Friedrichs-Lewy
DFSBC	Dynamic free surface boundary condition
KFSBC	Kinematic free surface boundary condition
MQ	Multiquadric
MQRBF	Multiquadric radial basis function
NMLI	Nonlinear model with linear input
NMNI	Nonlinear model with nonlinear input
NS	Navier Stokes
PDE	Partial differential equation
PDECB	Partial differential equation collocation on the boundary
RBC	Radiation boundary condition
RBF	Radial basis function

1. INTRODUCTION

1.1. Wave Modeling in General

The optimum utilization of the world's coastal zones relies heavily on the understanding of processes that play a role in the evolution of coasts in response to the forces of nature or human intervention. Of the natural forces, those due to waves are amongst the most important ones since waves gather energy and momentum from winds blowing over large ocean surfaces and transport them to the coast where they shape the coastal zone. Thus, the generation, propagation and transformation of waves have attracted researchers for more than a century. Along with field and laboratory studies of waves, analytical and numerical models of waves have been developed.

Each model depends on the approach how to treat the water as a material, the geometry of interested domain and certain characteristics involved in the wave propagation phenomena. A detailed account of wave theories and models can be found in texts such as those by Dingemans (1997a; 1997b), Kowalik and Murty (1993), Mei (1989). Out of these, there are models treating water as viscous therefore trying to simulate the wave propagation behavior through a set of equations that takes momentum and viscosity into account. Such models are called Navier-Stokes (NS) models owing its name to the field equation used in the model. However, analytical solutions to NS models can be obtained under some specific conditions. There is still ongoing research on NS models to apply it to a more general fluid flow. On the other side there are several inviscid models which can be classified as models of Laplace equation origin because the governing field equation contains the Laplacian of the velocity potential that can be identified in the absence of viscosity. The simplest of these is the linear wave theory based on the small wave amplitude oscillation and small wave steepness assumptions. In fact simplifications due to these assumptions remove the difficulties inherent in the boundary conditions defined at the surface. Further attempts to simulate more general conditions are realized by the introduction of higher order expansions of the field parameter such as in the Stokes wave theories and cnoidal wave theory. Since

these are approximate analytical theories, they have certain limitations. Parallel to these analytically approximate models, there are numerical models that try to find the coefficients of the higher order expansion of the field parameter to make it applicable to more general situations. Another group of models are the purely numerical ones. These using a certain technique try to solve the problem approximately. These techniques make it possible to obtain results of more complicated problems compared to the present analytical solutions. Some of these techniques through the use of known local functions try to simulate the unknowns at the locations or on certain elements obtained via domain or boundary discretization. However, performance of these numerical techniques even the most traditional ones are highly dependent on the locations that are predetermined to set up equation system of the model. Also, the order and the known function itself are important to construct a solution. Thus, researchers tend to develop more flexible methods to deal with problems with complicated or deforming geometry. The so-called mesh free methods are devised to answer these necessities.

Over the last couple of decades, mesh free methods have begun to emerge. Of these, the radial basis function (RBF) collocation method introduced by Kansa (1990a; 1990b) is one of the most promising. This method achieves greater accuracy by the collocation at the locations scattered throughout the domain. Moreover, the locations of the collocation points may be random in nature compared to regular mesh requiring methods. This flexibility of the collocation points is especially useful in moving or deforming boundary problems.

The aim of the present study is to investigate the viability of the RBF collocation method in the development of a numerical model for the solution of the classical wave boundary value problem. As such, the model should be able to accept as input any unknown solution (linear or nonlinear) of the wave boundary value problem and to propagate it without amplitude or phase error.

The model development was carried out in three phases. In the first phase, the model developed was based on the linearized version of the wave boundary value problem and was solved using linear wave theory input. In the second phase, the model was

modified for the nonlinear free surface boundary conditions. This required the introduction of a method to update the position of the free surface and the corresponding boundary conditions as the wave propagates. The model was run using a linear wave input which represents the lowest order nonlinear input. In the last phase of the development, the model was run using nonlinear input obtained from the stream function wave theory.

1.2. Irrotational Wave Propagation

One particular class of models that makes use of the potential flow theory, realizes the assumption that the velocity field can be derived from a scalar potential such as in Equation 1.1 below,

$$\mathbf{u} = \langle u, v, w \rangle = \boldsymbol{\nabla}\phi \tag{1.1}$$

where $\mathbf{u} = \mathbf{u}(x, y, z, t)$ or component-wise $\langle u(x, y, z, t), v(x, y, z, t), w(x, y, z, t) \rangle$ denotes the velocity field and ϕ denotes velocity potential in Cartesian coordinates. It is a known fact that viscosity generates vorticity which is initially generated at the bottom and surface boundaries. Since diffusion of vorticity from the boundaries to the interior is quite slow as shown by Longuet-Higgins (1953; 1960), neglecting viscosity and assuming the irrotational flow up to the breaking point may be a good approximation. This implies that the change in wave energy is negligibly small. Also since the dissipation of wave energy is excluded, it can be concluded that the wave amplitude does not attenuate and the wave number or frequency does not change. Hence inviscid, irrotational, frictionless are the definitions that can be used interchangeably and the corresponding governing equation is the so-called Laplace Equation as shown in Equation 1.2 below

$$\nabla^2\phi = 0 \tag{1.2}$$

where ϕ is the velocity potential. The governing equation is a second order linear partial differential equation(PDE) whose solution requires the specification of appropriate

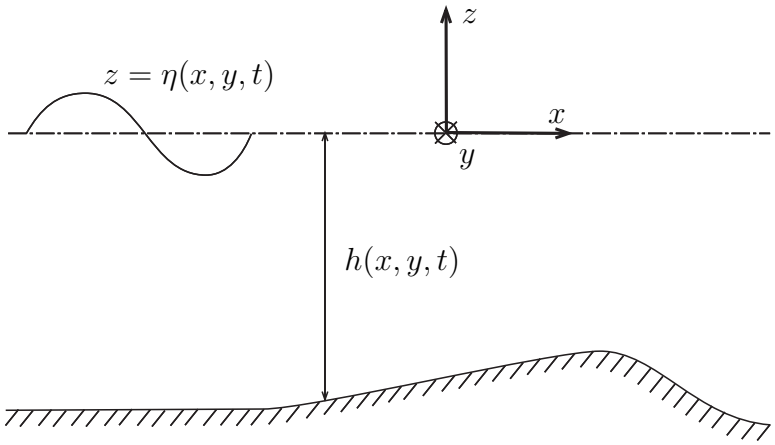

Figure 1.1. An illustration of wave boundary value problem

boundary conditions. Therefore, boundary conditions of this elliptic problem determine the characteristics of the solution and thus definition of them is a very important task to describe the expected flow. An illustrative problem geometry in a vertical section is given in Figure 1.1. Although not shown in the figure, in addition to the surface and bottom, four vertical lateral boundaries limit the domain both along x and y. Free surface can be expressed as a function of the horizontal spatial coordinates and time, namely $\eta(x, y, t)$. Similarly $h(x, y, t)$ denotes the position of the bottom usually with respect to an origin placed at the mean water level or at a certain elevation from a fixed datum. For the purpose of this study the waves will be considered to be of infinite crest length and as a consequence the y-direction (transverse to the direction of wave propagation) will be excluded. In the direction of wave propagation, the solution domain is delimited by two vertical boundaries extending over the depth. The up-drift boundary will be used for the specification of the forcing while on the down-drift boundary those conditions necessary to ensure purely outgoing waves will be specified. Since there are no objects or restrictions in the simulations of this study, the figure does not contain any object which may exist in a flow field. Also, in order to avoid going beyond the aim of this study, only those boundary conditions related with a two dimensional problem are discussed below.

1.2.1. Bottom Boundary Condition

There are several factors that have to be considered for the specification of the bottom boundary condition for an inviscid fluid. First of all it is important to know whether the boundary is fixed or moving. Except in rare cases, the bottom boundary is accepted as a fixed boundary. The next factor is the permeability of the bottom. If the bottom is permeable or at least if its permeability considerably affects the flow, then it is an important factor to consider. Finally, bottom geometry is another important factor that has to be accounted for. In general, the normal component of fluid velocity needs to be equal to the sum of the normal velocity of the boundary and the normal seepage velocity through it. This is shown below in Equation 1.3.

$$\mathbf{u} \cdot \mathbf{n} = u_b + u_s \tag{1.3}$$

where $\mathbf{n}$ is the surface normal, u_b is normal velocity of the bottom boundary and u_s is the normal component of the seepage through the boundary. Let the water depth is expressed as $h(x, y, t)$ as shown in Figure 1.1. Then, the bottom surface can be expressed as

$$z = -h(x, y, t) \tag{1.4}$$

or by surface

$$f_b(x, y, z, t) = z + h(x, y, t) \tag{1.5}$$

from here it follows that time rate of change of this surface vanishes if there is no seepage through this surface, i.e.

$$\frac{Df_b}{Dt} = 0 \tag{1.6}$$

or

$$-w = \frac{\partial h}{\partial t} + u\frac{\partial h}{\partial x} + v\frac{\partial h}{\partial y} \tag{1.7}$$

where u,v and w are the velocity components as introduced before. If the bottom boundary is fixed, time rate of change of depth vanishes so that the bottom boundary condition can expressed in the form

$$-w = u\frac{\partial h}{\partial x} + v\frac{\partial h}{\partial y} \tag{1.8}$$

One other possible case here is that bottom boundary can be horizontal and straight. Then fixed, impermeable and horizontal bottom boundary condition becomes

$$w = 0 \tag{1.9}$$

1.2.2. Free Surface Boundary Condition(s)

The free surface boundary condition can either be represented as two independent coupled conditions or as a combined condition. One of these independent coupled equations is the so-called dynamic free surface boundary condition. This is the unsteady Bernoulli Equation combined with the dynamic condition that includes atmospheric pressure and surface tension. The other one is the kinematic free surface boundary condition which is a result of the assumption that a particle on the free surface remains on the free surface. In fact, this assumption is realized neglecting micro-scale effects such as net transport of vapor and salt molecules causes the particles leave the surface. Therefore surface particles remain intact at the surface and move tangential to the surface. Written with respect to an Eulerian frame, equations below are the kinematic free surface (KFSBC) and dynamic free surface boundary conditions (DFSBC)

respectively.

$$\frac{\partial \eta}{\partial t} + u\frac{\partial \eta}{\partial x} + v\frac{\partial \eta}{\partial y} = 0 \qquad \text{at} \qquad z = \eta(x, y, t) \tag{1.10}$$

$$\frac{\partial \phi}{\partial t} + \frac{1}{2} \mid \boldsymbol{\nabla}\phi \mid^2 + \frac{p}{\rho} + g\eta = C'(t) \qquad \text{at} \qquad z = \eta(x, y, t) \tag{1.11}$$

where $\eta(x, y, t)$ is the free surface displacement, p is the pressure term containing atmospheric pressure and the surface tension at the free surface, $C(t)$ is the time dependent Bernoulli constant and g is the gravitational acceleration. When the pressure at the free surface is the ambient pressure of the air above the surface and the free surface does not possess large curvatures as a result of very short waves, the pressure term drops out of the DFSBC by setting the ambient pressure to zero. Even under these assumptions, the free surface boundary conditions preserve their nonlinearity which is always an issue unless small amplitude oscillations can be assumed.

In the case of small amplitude oscillation, given the amplitude of the wave is a, the order of magnitude of some characteristic parameters a/L and a/h are much less than unity. That is, if O denotes the order of its argument,

$$O(\frac{a}{L}) << 1 \qquad \text{and} \qquad O(\frac{a}{h}) << 1 \tag{1.12}$$

where L is the wave length and h is the water depth. This implies that higher order terms expressed in terms of a/L are much smaller and can be neglected. Another implication is that the free surface parameters can be expressed in terms of their value at the mean water level which is a direct result of expanding free surface parameters about the mean water level using Taylor's expansion and dropping out the negligible higher order terms. This also means that the mean water level is stationary so that the free surface boundary is treated as fixed and becomes easier to deal compared to a deforming boundary.

If nonlinear terms were to remain, then the forms of the free surface boundary conditions expressed in an Eulerian frame are difficult to model due to their non-

linearity. One other difficulty arises when the surface elevation becomes multivalued in the case of overturning and irrotationality is still accepted to exist instead of a dissipative model that deals with the wave breaking in more detail. During modeling, this is however not always a desired situation because breaking or overturning of waves involves energy dissipation that cannot be neglected. However, in practice when wave overtopping and wave loads on structures are calculated, the wave front geometry is particularly required. To overcome these difficulties, Longuet-Higgins and Cokelet (1976) introduced Lagrangian variables to keep track of the surface particles in time and extract information from their positions for the coincident Eulerian surface necessary to calculate the velocity field.

If a surface particle at a position (x_0, z_0) starts its motion at time t_0, its position (x, z) at a later time t in the Lagrangian view becomes

$$x = x_0 + \int_{t_0}^{t} u_L(x_0, z_0, t)dt \tag{1.13}$$

$$z = z_0 + \int_{t_0}^{t} w_L(x_0, z_0, t)dt \tag{1.14}$$

where $u_L(x_0, z_0, t)$ and $w_L(x_0, z_0, t)$ are the Lagrangian velocity components of the particle along the horizontal and vertical respectively. Hence, at the instant t the Eulerian surface passing through (x, z) will have the same velocities and potentials as that of the Lagrangian particle. It has to be noted here that although positions of the particles will determine several points of the surface passing through them during the numerical implementation of the approach, the medium can still be treated as a continuum. This is how a continuous Eulerian surface is numerically obtained from the positions of Lagrangian particles. Therefore, instead of the free surface boundary conditions specified with respect to an Eulerian frame in Equations 1.10 and 1.11, the following set of equations can be used.

$$\frac{Dx_L}{Dt} = u_L \tag{1.15}$$

$$\frac{Dz_L}{Dt} = w_L \tag{1.16}$$

$$\frac{D\phi_L}{Dt} = \frac{1}{2}\left|\boldsymbol{\nabla}\phi_L\right|^2 - gz_L \tag{1.17}$$

Here, x_L and z_L are the Lagrangian positions of the particles, ϕ_L is the Lagrangian potential of a particle and u_L and w_L are the velocity components along the horizontal and the vertical respectively. This approach is sometimes referred to as the fully Lagrangian descriptions of the surface. This description keeps track of the movement of surface particles along both vertical and horizontal. However, it is possible to keep track of only the vertical movement of the surface at a fixed horizontal position as seen in the study by Kennedy and Fenton (1996; 1997) and Fenton and Kennedy (1996) and this approach is called semi-Lagrangian approach. Again expressed in two dimensions, the surface velocity potential at a fixed point x_f in the horizontal also depends on the vertical coordinate and time, i.e.

$$\phi_s = \phi(x_f, z, t) \qquad \text{on} \qquad z = \eta \tag{1.18}$$

where η corresponds to the free surface displacement. And its time rate of change becomes,

$$\frac{\partial \phi_s}{\partial t} = C'(t) - g\eta - \frac{1}{2} \mid \boldsymbol{\nabla}\phi \mid^2 + \frac{\partial \phi}{\partial z}\frac{\partial \eta}{\partial t} \qquad \text{on} \qquad z = \eta \tag{1.19}$$

This equation is used coupled with the KFSBC introduced before in Equation 1.10 to keep track of the change of the free surface in the vertical at a fixed position along the horizontal. It has to be noted here that the semi-Lagrangian description also lacks the capability to simulate overturning like the fully Eulerian expressions of the free surface boundary conditions introduced before in Equations 1.10 and 1.11.

1.2.3. Truncation Boundary Conditions

These boundary conditions are used for a complete definition of the problem. Concentrating on the case that there are no objects or obstacles in the domain where a local boundary condition specification would be necessary, it can be assumed that there are only outgoing waves at the infinity. This assumption requires a radiation boundary condition(RBC) at the outflux section of the domain. However, since it is not practical to simulate at infinity, the boundary is truncated and a radiation boundary condition is

applied at some distance from the influx section in order to approximate the behavior at infinity. At the influx section any kind of suitable boundary condition that carries the information about the propagating wave can be used. For example the following conditions are the most conventionally used Dirichlet and Neumann type boundary conditions respectively.

$$\phi = \phi_i(x_0, z, t) \tag{1.20}$$

$$\frac{\partial \phi}{\partial x} = u_i(x_0, z, t) \tag{1.21}$$

where ϕ_i is the input wave potential and u_i is the input water particle velocity at the position of the influx boundary with its normal along x, say at $x = x_i$.

There are also other ways to treat the radiation boundary by using the so-called absorbing boundary condition. One possibility here is that if the waves are periodic in space and time, one can make use of periodic boundary conditions. For example if Dirichlet type of boundary condition is going to be used, periodic boundary condition in both space and time is

$$\phi(x, t) = \phi(x + L, t) \tag{1.22}$$

$$\phi(x, t) = \phi(x, t + T) \tag{1.23}$$

where L and T are the wave length and the wave period respectively. In the study by Longuet-Higgins and Cokelet (1976), the periodic boundary condition is used to transform the free surface into a circle for use in the boundary integral method. Another way of introducing absorbing boundary condition is by selection of the boundary far away from the area of interest. This way the wave field can be correctly predicted until the reflected waves spoil the solution. However, this means a simulation time limitation as in Isaacson (1982). As can be seen in the study by Israeli and Orszag (1981), some damping term, which works like a sponge filter, can be added to the PDE to simulate the absorbing boundary. Yet another technique is to use simple outer field solutions at the boundary. For instance, Lin et al. (1984) used linear waves outside the field

for nonlinear computations inside the domain of interest. A widely used approach to the absorbing boundary is through the use of a PDE as in Sommerfeld (1949) where a scattering wave potential and thus the wave amplitude are shown to vanish for the radial distance going to infinity. Sommerfeld's radiation boundary condition when time dependence and only outgoing waves are present takes the form below.

$$\frac{\partial \phi_s}{\partial r'} + \frac{1}{C}\frac{\partial \phi_s}{\partial t} = 0 \tag{1.24}$$

where ϕ_s is the potential of the scattering wave field along a radial distance r', and C is the phase speed of the waves. This form is the first order and normally incident case of the higher order non-reflecting boundary condition proposed by Higdon (1986; 1987) as shown below.

$$\left(\frac{C_0}{\cos\theta_n}\frac{\partial \phi_s}{\partial r} + \frac{\partial}{\partial t}\right)_o^n \phi_s = 0 \tag{1.25}$$

where C_0 is the linear phase speed, θ_n is the angle between the boundary normal and the direction of outgoing waves and n_o is the order of accuracy. And it is clear that Sommerfeld's condition corresponds to case where $n = 1$ and $\theta_n = 0$. Higdon (1986; 1987) is in fact a generalization of the boundary conditions presented by Engquist and Majda (1977). In their study, Engquist and Majda (1977) developed a local boundary condition that minimizes the reflection. These conditions are practical compared to nonlocal conditions which are difficult to use in numerical applications. However, one particular disadvantage of these studies is that they assumed that the wave form is available at hand. Broeze and Van Daalen (1992), without using a priori knowledge about the form of the waves, derived a boundary condition using variational principles and obtained improved accuracy in the panel method. A numerical approach to Sommerfeld's boundary condition was used in Orlanski (1976) where the phase speed of the wave is numerically calculated in the vicinity of the boundary and this condition has started to be called the Sommerfeld/Orlanski boundary condition. A detailed account of the literature on these type of boundary conditions can be found in Romate (1989).

1.3. Linear Wave Theory

A linear solution to the wave propagation problem, can be obtained through linearization of the free surface boundary conditions. As stated before in Equation 1.12, if the characteristic arguments a/L and a/h are very small, then higher order terms in the free surface boundary conditions vanish because they lead to much more smaller values. As illustrated in the Figure 1.2, the two dimensional periodic water wave boundary problem solution which can be found in most wave mechanics text books such as the one by Dean and Dalrymple (1984), is given. Since the wave is periodic in space and time, one wavelength is taken under consideration. The bottom is impervious and horizontal and the surface tension is neglected. Also ambient air pressure above the free surface is taken to be zero. The linearized KFSBC and DFSBC at the mean water level are respectively given below.

$$\frac{\partial \eta}{\partial t} = -\frac{\partial \phi}{\partial z} \qquad \text{on} \qquad z = 0 \tag{1.26}$$

$$\frac{\partial \phi}{\partial t} = g\eta \qquad \text{on} \qquad z = 0 \tag{1.27}$$

The time dependent Bernoulli constant vanishes because there is no change in the mean water level. The small amplitude assumption lets these boundary conditions to be written at the mean water level. In addition, the bottom boundary condition for a horizontal and impervious bottom is expressed as

$$\frac{\partial \phi}{\partial z} = 0 \qquad \text{on} \qquad z = -h \tag{1.28}$$

and the lateral periodicity conditions are already given in Equations 1.22 and 1.23. Under these conditions the Laplace equation is solved using the method of separation of variables. Depending on the selections it is possible to obtain the free surface displacement in space x and time t, such as

$$\eta(x,t) = \frac{H}{2}\cos(kx - \omega t) \tag{1.29}$$

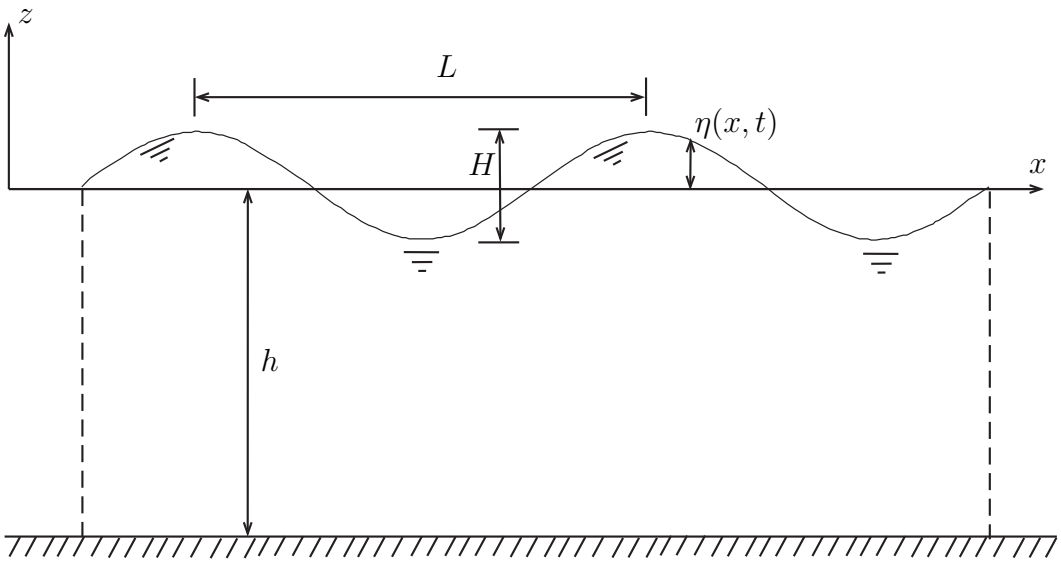

Figure 1.2. Some two dimensional periodic wave characteristics

where H is the wave height, k is the number of waves per unit length or wavenumber and ω is the wave angular frequency. Then, the corresponding velocity potential is

$$\phi(x,z,t) = -\frac{H}{2}\frac{g}{\omega}\frac{\cosh k(h+z)}{\cosh kh}\sin(kx-\omega t) \tag{1.30}$$

1.4. Stream Function Wave Theory

The analytical solution for linear waves is restricted mainly by the smallness of the wave steepness. This has led to development of theories where the small wave steepness criterion is relaxed so that waves of "finite amplitude" are obtained using the nonlinear boundary conditions at the free surface. Recently after Airy's (1845) work in which the solution to the linear problem is given for the first time, higher order analytically approximate expansions were proposed in the study by Stokes (1847). Several other nonlinear higher order approximations such as cnoidal theory have been proposed to model more general waves found in the nature. However, all these approximations also have some limitations in their applicability. Stokes theory assumes that the variation in the horizontal can be expressed in terms of a Fourier series and the coefficients of these series are expressed as perturbation expansions in terms of wave amplitude. Calculation of these coefficients is a very tedious task so that the orders up to which

these coefficients are calculated are not always accurate enough that this theory breaks down in shallow water and high waves. In order to get more accurate results, instead of using perturbation expansions, coefficients of the Fourier series can be determined using numerical techniques to solve a nonlinear set of equations formed accordingly. In the study (Dean, 1965), the stream function solution of the Laplace equation that satisfies the bottom boundary condition was used. The best possible coefficients fitting the KFSBC and the DFSBC were calculated using a nonlinear least squares method. On the other hand Rienecker and Fenton (1981) utilized the stream function to construct a set of equations which are then solved by nonlinear Newton method to calculate the coefficients approximating nonlinear steady waves. In the study by Rienecker and Fenton (1981), entries of the Jacobian matrix are computed exactly. In a more recent study by Fenton (1988), the entries of the Jacobian matrix are calculated using numerical derivatives. Fenton (1988) removed the difficulties due to the calculation of the Jacobian matrix inherent in the study by Rienecker and Fenton (1981) so that it is applicable to more general situations.

According to Fenton (1988), the horizontal and vertical velocity components with respect to a stationary physical frame were obtained as

$$u(x,z,t) = C - \overline{u} + (g/k)^{1/2} \sum_{j=1}^{N_s} jB_j \frac{\cosh jk(h+z)}{\cosh jkh} \cos jkx \tag{1.31}$$

$$v(x,z,t) = (g/k)^{1/2} \sum_{j=1}^{N_s} jB_j \frac{\sinh jk(h+z)}{\cosh jkh} \sin jkx \tag{1.32}$$

Here C is the wave velocity, B_j are the unknown coefficients, k is the wave number of the primary mode, $\overline{u}$ is the mean fluid speed relative to wave and N_s, being one less than the number of points at which free surface displacements are calculated, is the order of the stream function.

1.5. Numerical Methods

The wave propagation problem may also be solved using numerical methods. Among others, numerical methods commonly used are the finite difference method, the

finite element method, the finite volume method, and the boundary element method. The first three can be classified as domain discretization methods using a mesh of nodal points, area or volume elements generated so that they conform to the problem boundaries. The boundary element method has the advantage that when applied to the solution of linear PDEs requires meshing only on the curve or surface bounding the solution domain. However, when the governing equation is nonlinear, integration within the solution domain is required and the method formulation is revised so that these integrals may be transformed to the boundary. This process involves nodes within the solution domain. When the solution of a problem involving deformable boundaries is required, all methods with the exception of the boundary element method are difficult to use as the solution domain boundaries are part of their meshes which were originally generated using certain rules. Although it is possible to speak of certain guidelines in forming a boundary mesh for the boundary element method, in general the placement and subsequent movement of boundary nodes is relatively simple. Overall, regardless of the nature of the mesh required by a particular technique, meshing is a time consuming effort that detracts the modeler from his efforts in developing a code that better represents the physics of the problem at hand. To avoid meshing, the last decade witnessed the development of meshless methods; meshless in the sense that the rules of computational node placement are very few and flexible.

RBFs denoted by $\varphi(\|x - x_j\|)$ or sometimes by $\varphi(r)$, are functions that depend on the distance between nodes x and x_j such that $x \in \Re^n$ and $x_j \in \Re^n$ in n dimensions. This is a scalar multivariate function dependent on the norm of its argument, i.e. φ depends on $r = \|x - x_j\|$. As its definition suggests, an RBF is a function radially symmetric about x_j so that x_j are called centers or nodes. Some RBFs depend on a shape parameter c, and are then denoted as $\varphi(r, c)$. Commonly used RBFs found in the literature are tabulated in Table 1.1. It has to be noted here that all of the functions listed in Table 1.1 are functions with global support. For the sake of efficiency in computing matrix systems arising in a simulation problem, other RBFs with compact support are also available. In order to illustrate, Wendland's positive definite compactly supported functions are tabulated in Table 1.2 as in (Wendland, 1995).

Table 1.1. Some commonly used RBFs with global support

Piecewise Smooth RBFs	$\varphi(r)$
Piecewise Polynomial	$\|r\|^n$, n odd
Thin Plate Spline	$\|r\|^n \ln \|r\|$, n even
Infinitely Smooth RBFs	$\varphi(r, c)$
Multiquadric(MQ)	$\sqrt{r^2 + c^2}$
Inverse Multiquadric	$\frac{1}{\sqrt{r^2+c^2}}$
Gaussian	e^{-cr^2}

Table 1.2. Wendland's positive definite functions with compact support

Dimension	$\varphi(r)$	Smoothness
1	$(1-r)$	C^0
	$(1-r)_+^3(3r+1)$	C^2
	$(1-r)_+^5(8r^2+5r+1)$	C^4
2	$(1-r)_+^2$	C^0
	$(1-r)_+^4(4r+1)$	C^2
	$(1-r)_+^6(35r^2+18r+3)$	C^4
	$(1-r)_+^8(32r^3+25r^2+8r+1)$	C^6

In Table 1.2 + operator is used to express $\varphi(r)$ as a univariate polynomial $p'(r)$ or 0 depending on the values of r. Clearly,

$$\varphi(r) = \begin{cases} p'(r) & \text{if } 0 \leq r < 1 \\ 0 & \text{if } r > 1 \end{cases} \tag{1.33}$$

Utilization of RBFs roots back to the approximation of scattered n dimensional data that is not necessarily located on a regular grid so that the methods using these global functions to recover data using the pairwise distances between the centers at which the data is located are called meshless methods. In other words, using N distinct locations $x_1, \ldots, x_N \in \Omega \subset \Re^n$ at which the values $y_1, \ldots, y_N$ are defined, one can construct a linear combination

$$f(\mathbf{x}, c) = \sum_{i=1}^{N} \alpha_i \varphi(\|x - x_j\|, c) \tag{1.34}$$

which best fits the data $\{x_i, y_i\}$ for $i = 1, 2, \ldots, N$. This combination is obtained by solving a simultaneous set of equations as

$$\mathbf{\Phi}\boldsymbol{\alpha} = \mathbf{y} \tag{1.35}$$

Here the, NxN coefficient matrix $\mathbf{\Phi}$ is composed of entries Φ_{ij} given by

$$\Phi_{ij} = \varphi(\|x_i - x_j\|, c), \qquad \text{where} \qquad i, j = 1, 2, \ldots, N \tag{1.36}$$

$\boldsymbol{\alpha}$, the vector of coefficients is of length N and has the elements α_i. The values y_i form the elements of vector $\mathbf{y}$ also of length N. The interpolant given in Equation 1.34 may also be augmented by using polynomials $p_k(x)$ of order M_a, that is

$$f(\mathbf{x}, c) = \sum_{i=1}^{N} \alpha_i \varphi(\|x - x_j\|, c) + \sum_{j=1}^{M_a} \beta_k p_k(x) \tag{1.37}$$

The form given in Equation 1.37 has now $N + M_a$ unknown coefficients implying an

underdetermined system matrix of $N\text{x}(N + M_a)$. Here necessary M_a more equations can be obtained by requiring

$$\sum_{j=1}^{N} \alpha_j p_i(x_j) = 0 \qquad i = 1, \ldots, M_a \tag{1.38}$$

In this case the system matrix becomes,

$$\mathbf{\Phi}' = \begin{bmatrix} \mathbf{\Phi} & \mathbf{P} \\ \mathbf{P^T} & 0 \end{bmatrix} \tag{1.39}$$

where $\mathbf{P}$ is the N by M_a matrix with entries $P_{ij} = p_j(x_i)$ and $\mathbf{P^T}$ is the transpose of $\mathbf{P}$. And the resulting system of equations become,

$$\begin{bmatrix} \mathbf{\Phi} & \mathbf{P} \\ \mathbf{P^T} & 0 \end{bmatrix} \begin{Bmatrix} \mathbf{\Phi} \\ \boldsymbol{\beta} \end{Bmatrix} = \begin{Bmatrix} \mathbf{y} \\ \mathbf{0} \end{Bmatrix} \tag{1.40}$$

The choice of augmentation is left to the modeler depending on the requirements of the problem, because no proof is present that supports its usage. The rest of this text will only deal with the non-augmented form.

During the interpolation process, the most important issue a modeler will face is the invertibility of the coefficient matrix. As pointed out in related texts, for example in the text by Buhmann (2003), the solvability of the system in Equation 1.35 is guaranteed if the quadratic form

$$\boldsymbol{\alpha^T \Phi \alpha} = \sum_{i=1}^{N} \sum_{j=1}^{N} \alpha_i \alpha_j \varphi(\|x_i - x_j\|, c) \tag{1.41}$$

is strictly positive when the vector of interpolation coefficients $\boldsymbol{\alpha}$ is different than $\mathbf{0}$ and data points are distinct. Moreover, this positive definiteness requirement for solvability is guaranteed if the function $\varphi(\|x_i - x_j\|, c)$ is strictly completely monotonic.

In particular, Hardy (1971) used the multiquadric radial basis function (MQRBF) to interpolate topographical surfaces in a technique very similar to the technique introduced above. Franke (1982) showed that Hardy's MQ method was the best among the 29 different algorithms used for the interpolation of scattered data. A more recent study by Kansa (1990a) underlines the MQ method's success and ease of its applicability as long as scattered data interpolation is concerned. Kansa (1990b) dealt with the application of MQ method to the solution of PDEs and stated that the method can be applied to linear or nonlinear hyperbolic, elliptic, parabolic equations. Some attractive properties of the MQRBF can be listed as follows:

- Continuously differentiable.
- Integrable.
- Capable of representing functions with steep gradients with very high accuracy.
- Better approximations can be obtained via adjusting the shape parameter.
- Exponential error convergence rate, (Madych and Nelson, 1990).

The shape parameter, which need not be constant is a key factor that affects the solvability and accuracy of the method in that it affects the condition number of the system matrix. Apart from the effect of the distance between two centers which leads to approximately same rows of those centers when they are too close, selection of the shape parameter is also important. MQs with shape parameters large in value generate more flat functions and functions with small shape parameters are more cone like. In order to get a better conditioned matrix, Kansa (1990b) used a variable shape parameter that gives exponential variation. Golberg et al. (1996) used a statistical procedure that optimizes for an efficient shape parameter. In some studies conventional values or ranges for the shape parameter are given, see for example Hon et al. (1999). Most of the time optimum shape parameter is expressed in terms of the average, maximum or minimum values of the distances between the centers.

When a boundary value problem is defined, the approach to determine the unknown coefficients depends on the preferences of the modeler and the complexity of the problem. However owing to its easiness, collocation is the most common technique

preferred by researchers. Here, three different collocation techniques applied to an n dimensional linear elliptic problem, are presented as the nature of the target problem of the study suggests. On an n dimensional domain Ω such that $\Omega \subset \Re^n$ with the boundary $\partial\Omega$, the following problem can be posed.

$$L_o s_u(\mathbf{x}) = f(\mathbf{x}) \qquad \text{in} \qquad \Omega \tag{1.42}$$

$$B_o s_u(\mathbf{x}) = g_o(\mathbf{x}) \qquad \text{on} \qquad \partial\Omega \tag{1.43}$$

where L_o and B_o are the field and boundary operators respectively. Let the first N of the $N+M$ centers selected lie inside the domain, namely $x_i \subset \Omega$ for $i = 1, \ldots, N$ and the rest on the boundary such that $x_i \subset \partial\Omega$ for $i = N+1, \ldots, N+M$.

The first technique is the direct collocation method that assumes the approximate interpolant $s(\mathbf{x}, c)$ for the unknown $s_u(\mathbf{x})$. As such

$$s(x_i, c) = \sum_{j=1}^{N+M} \alpha_j \varphi(\|x_i - x_j\|, c) \tag{1.44}$$

and its collocations at the interior and boundary centers respectively are

$$L_o s(x_i, c) = \sum_{j=1}^{N+M} \alpha_j L_o \varphi(\|x_i - x_j\|, c) = f(x_i) \qquad i = 1, \ldots, N \tag{1.45}$$

$$B_o s(x_i, c) = \sum_{j=1}^{N+M} \alpha_j B_o \varphi(\|x_i - x_j\|, c) = g(x_i) \qquad i = N+1, \ldots, M \tag{1.46}$$

The resulting system matrix is unsymmetrical and a representation of the system can be given as

$$\left[\frac{L_o\varphi}{B_o\varphi}\right]\{\boldsymbol{\alpha}\} = \left\{\frac{f}{g}\right\} \tag{1.47}$$

The straight collocation technique is the one used in all of the problems solved in this study. Also, it has to be noted that since the system matrix is unsymmetric, invertibility is not guaranteed and the selection of the shape parameter is quite important.

In order to guarantee nonsingularity, a symmetric system of equations is constructed in the second technique. The idea behind the symmetric collocation technique is that the field operator is used at the centers corresponding to the interior points and the boundary operator at the boundary centers in the definition of the interpolant and the system is set up using this modified interpolant as shown below.

$$s(x_i, c) = \sum_{j=1}^{N} \alpha_j L_o \varphi(\|x_i - x_j\|, c) + \sum_{j=N+1}^{N+M} \alpha_j B_o \varphi(\|x_i - x_j\|, c) \tag{1.48}$$

and the corresponding collocation set of equations are,

$$\begin{aligned} L_o s(x_i, c) &= \sum_{j=1}^{N} \alpha_j L_o^2 \varphi(\|x_i - x_j\|, c) + \sum_{j=N+1}^{N+M} \alpha_j L_o B_o \varphi(\|x_i - x_j\|, c) \quad (1.49) \\ &= f(x_i) \qquad i = 1, \ldots, N \\ B_o s(x_i, c) &= \sum_{j=1}^{N} \alpha_j B_o L_o \varphi(\|x_i - x_j\|, c) + \sum_{j=N+1}^{N+M} \alpha_j B_o^2 \varphi(\|x_i - x_j\|, c) \quad (1.50) \\ &= g(x_i) \qquad i = N+1, \ldots, N+M \end{aligned}$$

A schematic representation of the system for this case can also be given as

$$\left[\begin{array}{c|c} L_o^2 & L_o B_o \\ \hline B_o L_o & B_o^2 \end{array}\right] \{\boldsymbol{\alpha}\} = \left\{\begin{array}{c} f \\ \hline g \end{array}\right\} \tag{1.51}$$

Hence, the system matrix becomes symmetrical.

Since the errors near the boundaries are largest as shown in the study by Fornberg et al. (2002), Fornberg et al. (2002) developed the third approach, namely the PDE collocation on the boundary(PDECB) method which not only collocates boundary conditions but also the field equation at the boundary points. Applying the field equation to the boundary centers brings about new equations which necessitates an increase in the unknowns so that the authors took additional centers outside the boundary which they may have also taken inside. Let N' be the number of collocation centers both on the boundary and inside, i.e. $N' = N + M$. Then taking M additional centers outside

the boundary following interpolant is used to form the equations,

$$s(x_i, c) = \sum_{j=1}^{N'+M} \alpha_j \varphi(\|x_i - x_j\|, c) \tag{1.52}$$

and the corresponding system is

$$L_o s(x_i, c) = \sum_{j=1}^{N'+M} \alpha_j L_o \varphi(\|x_i - x_j\|, c) = f(x_i) \quad i = 1, \ldots, N' \tag{1.53}$$

$$B_o s(x_i, c) = \sum_{j=1}^{N'+M} \alpha_j B_o \varphi(\|x_i - x_j\|, c) = g(x_i) \quad i = N+1, \ldots, N+M \tag{1.54}$$

where the first N centers are inside the boundary followed by M centers on the boundary first, and additional M centers outside. The schematic representation for this technique is quite similar to that of the direct collocation technique except the number of equations.

For time-dependent problems, the evolution of the interpolant is achieved through the variation of coefficients in time. Hence, the general form of the interpolant given in Equation 1.34, is rewritten below taking the time variation into account. Since the RBF is only a spatial function, time variation is simply attributed to the coefficients.

$$s(\mathbf{x}, t, c) = \sum_{i=1}^{N} \alpha_i(t) \varphi(\|x - x_j\|, c) \tag{1.55}$$

Accordingly, time derivative of the interpolant becomes,

$$\frac{\partial s(\mathbf{x}, t, c)}{\partial t} = \sum_{i=1}^{N} \frac{\partial \alpha_i(t)}{\partial t} \varphi(\|x - x_j\|, c) \tag{1.56}$$

1.6. Initial Value Problem

When the problem at hand dictates that the solution evolves in time the solution technique is accordingly modified. The unsteady nature of the problem is accounted

for by introducing time dependency in the $\boldsymbol{\alpha}$-vector and by using appropriate time integration scheme. There are a number of self starting(single step) schemes such as Euler method, modified Euler method, Heun method, Runge-Kutta methods, Taylor polynomial method as well as multi-step methods such as Adams-Basforth method, Adams-Moulton method. However, since the predictor-corrector type equations uses past information they lack the ability to start initial value problems. Self-starting schemes are used at the beginning until information necessary for predictor-corrector schemes is produced. Also, there are extrapolation schemes such as Blurisch-Stoer method. These numerical schemes are cited in the related literature by Press et al. (1992), Burden and Faires (1993), Durran (1998). As a time integration method, fourth order Runge-Kutta method is used in this study because it is known to work well for smooth problems. Moreover, it is a self starting method so that the initial input will be sufficient to proceed in time. It involves 4 evaluations per time step and local truncation error is fourth order(Burden and Faires, 1993). Also, since the expected results are smooth, adaptive step size control is not deemed necessary. To construct an approximate solution to the initial-value problem

$$y' = f_d(t, y) \qquad a \leq t \leq b, \qquad y(a) = y_0 \tag{1.57}$$

the fourth order Runge-Kutta method poses the following for y at some time step $i+1$ using value of y at the step i.

$$y^{i+1} = y^i + \frac{1}{6}(k_1 + 2k_2 + 2k_3 + k_4) \tag{1.58}$$

where k_1,k_2,k_3 and k_4 are

$$k_1 = h f_d(t^i, y^i) \tag{1.59}$$

$$k_2 = h f_d(t^i + \frac{h}{2}, y^i + \frac{1}{2}k_1) \tag{1.60}$$

$$k_3 = h f_d(t^i + \frac{h}{2}, y^i + \frac{1}{2}k_2) \tag{1.61}$$

$$k_4 = h f_d(t^{i+1}, y^i + k_3) \tag{1.62}$$

in terms of the time step h.

2. WATER WAVE PROPAGATION PROBLEM

2.1. Objective and Scope

In this study the two dimensional irrotational wave propagation over a horizontal, fixed, impermeable bottom is numerically modeled using the unsymmetric MQ method. During the three different phases of the study, three different numerical models are developed. In all of the models the Sommerfeld radiation boundary condition is used and the shape parameter of the MQRBF is taken as constant. The first model differs from the others in two aspects. It is the linearized version of the wave propagation problem therefore it has some characteristics peculiar to linearization and therefore its numerical implementation is different. The other model use the fully nonlinear forms of the surface boundary conditions. To override the inherent difficulties in the fully nonlinear surface boundary conditions, mixed coordinate systems are used where the instantaneous boundary value problem is approximated in an Eulerian frame whereas the surface is evolved in a fully or semi Lagrangian frame. The second model uses fully Lagrangian descriptions to evaluate the evolution of the surface in time. Centers except those on the surface are stationary and the input wave is a linear cosine wave which can be used since the linear wave is a limiting case of nonlinear waves. The third model uses semi Lagrangian descriptions of the surface and can take a nonlinear stream function wave input. The positions of the collocation centers except the bottom nodes change in time. Time evolution is simulated using the fourth order Runge-Kutta method in all of the models. During the solution of the instantaneous boundary value problems at the surface and at the radiation boundary Dirichlet type boundary conditions are used and for the rest of the boundaries, namely at bottom and influx lateral boundary, Neumann type boundary conditions are used. All of the models are compared with the expected solutions and errors in the wave amplitude and phase speed are inspected. As a result in order to fulfill the purpose of this study, it is shown that MQ method is an efficient way to simulate the wave propagation phenomenon.

2.2. Assumptions

In the following, the assumptions for the problem at hand are summarized prior to the definition of the boundary value problem.

- The fluid is inviscid and incompressible.
- The flow is unsteady and irrotational.
- There is no generation or dissipation of wave energy. That is, energy is conserved.
- The waves have infinite crest length so that the problem is rendered two-dimensional.
- The bottom boundary is fixed, impervious and horizontal.
- The horizontal extent of the solution domain is truncated at a vertical section where wave radiation to infinity can be modeled using the Sommerfeld radiation condition.
- For the linear model the wave steepness is small, that is $O(ak) << 1$.
- The air pressure above the free surface is constant and is taken to be zero.

2.3. Problem Definition

According to the assumptions above, the problem can be defined on a domain Ω where boundaries are respectively as the surface, bottom, influx and radiation boundaries $\partial\Omega_s$, $\partial\Omega_b$, $\partial\Omega_i$, $\partial\Omega_r$. Here a Cartesian coordinate system, whose origin is placed at the mean water level of the entrance section as illustrated in the Figure 2.1 is used. To formulate the general problem to be solved, the classical problem is augmented by the radiation condition on $\partial\Omega_r$, the wave input on $\partial\Omega_i$, initial conditions for the wave potential of the free surface. The equations defining the problem are,

$$\nabla^2\phi = 0 \quad \text{in} \quad \Omega \tag{2.1}$$

$$\frac{\partial\phi}{\partial t} + g\eta + \frac{1}{2} \mid \boldsymbol{\nabla}\phi \mid^2 = 0 \quad \text{on} \quad \partial\Omega_s \tag{2.2}$$

$$\frac{\partial\eta}{\partial t} + \frac{\partial\phi}{\partial x}\frac{\partial\eta}{\partial x} - \frac{\partial\phi}{\partial z} = 0 \quad \text{on} \quad \partial\Omega_s \tag{2.3}$$

$$\frac{\partial\phi}{\partial z} = 0 \quad \text{on} \quad \partial\Omega_b \tag{2.4}$$

$$\frac{\partial \phi}{\partial t} + C\frac{\partial \phi}{\partial x} = 0 \qquad \text{on} \qquad \partial\Omega_r \tag{2.5}$$

$$\frac{\partial \phi}{\partial x} = u(x = 0, z, t) \qquad \text{on} \qquad \partial\Omega_i \tag{2.6}$$

$$\eta(x, t_0) = \eta_0 \qquad \text{on} \qquad \partial\Omega_s \tag{2.7}$$

$$\phi(x, z, t_0) = \phi_0 \qquad \text{on} \qquad \partial\Omega_s, \partial\Omega_r \tag{2.8}$$

where $\phi = \phi(x, z, t)$ is the velocity potential, $\eta = \eta(x, t)$ is the free surface displacement, C is the phase velocity of the wave main mode, ϕ_0 and η_0 are the initial values of the potentials and displacements at time t_0. The elliptic governing equation, namely Laplace's equation is given in Equation 2.1. The DFSBC and KFSBC are respectively given by Equations 2.2 and 2.3. Equation 2.4 is the no-flux condition defined at the impermeable bottom boundary. The information about the input wave is defined at the influx boundary with the condition Equation 2.6. The input wave information is carried downstream solving the boundary value problems at each time step of computation. Necessary initial values for the initial value problems at the surface are specified by Equations 2.7 and 2.8. The nonlinearity of the problem originates at the free surface boundary and a fairly simple approach to deal with the problem was addressed in the previous chapter. The Sommerfeld condition posed on the radiation boundary is given by Equation 2.5. Although at the beginning the models are developed using the Sommerfeld boundary condition, there was no clue about whether this condition works well for the fully nonlinear case or not. It is a well known fact that this first order condition only allows the fundamental mode of a wave to pass through the radiation boundary. Therefore as the nonlinearity increases, the efficiency of the Sommerfeld radiation boundary condition decreases. In order to meet the objective of the study periodic boundary condition is used alternatively. These conditions assume the velocity potential is periodic in space and time. Hence along a wavelength L, the influx and radiation boundary conditions are taken as,

$$\phi(x = L, z, t) = \phi(x = 0, z, t) \qquad \text{on} \qquad \partial\Omega_r \tag{2.9}$$

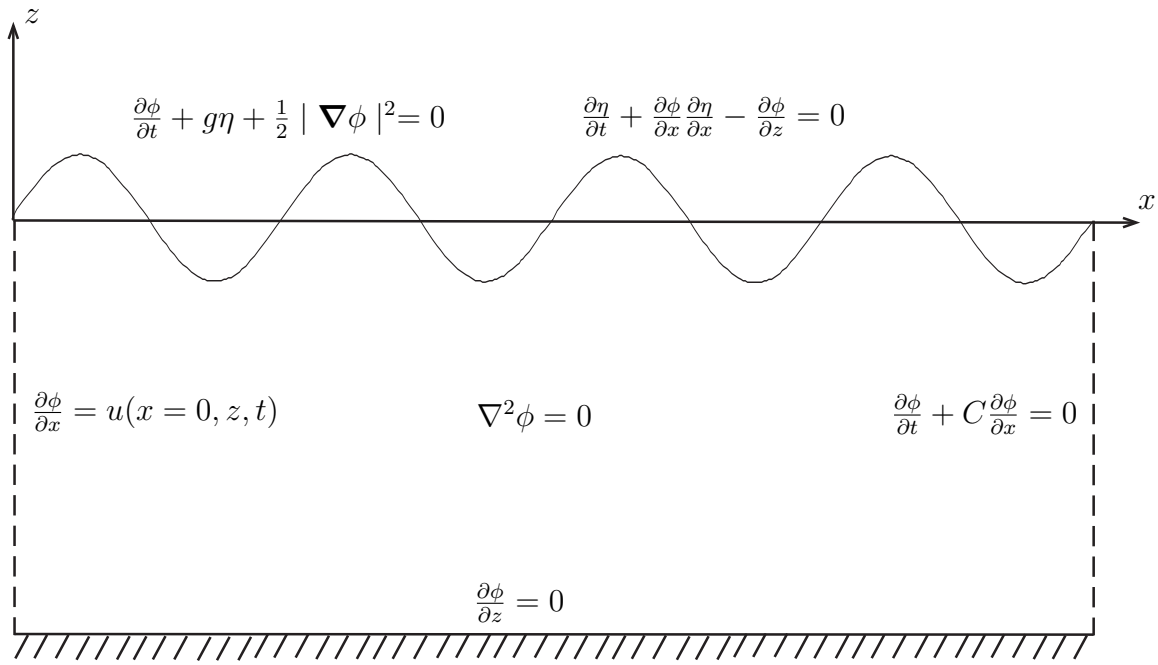

Figure 2.1. Two dimensional irrotational wave propagation over horizontal bottom

3. LINEAR WAVE PROPAGATION

3.1. Introduction

In the first phase of the study a numerical model for linear waves is developed to simulate the water wave propagation problem defined in the previous chapter. However, the effect of linearization is used so that instead of the full form of the nonlinear surface boundary conditions the linearized conditions are used. Due to this linearization, the numerical approach is simplified as the surface parameters can now be expressed in terms of their values at the stationary mean water level. Therefore, the problem geometry does not deform in time and thus computationally expensive boundary updating procedures which require inversion or linear system solution at each time step are avoided. In other words, once the positions of the centers are determined and the necessary system matrices are set up, they can be used in time without any change. Since the computational cost of the inversion process or linear system solution is considerably high in comparison to those of the other necessary numerical operations, the linear problem is easy to implement by requiring expensive procedures only once at the beginning. Also the difficulties associated with the nonlinear form do not exist in the linear case and the surface boundary conditions can be numerically simulated easily and without any other coordinate definition such as in the case of the mixed Lagrangian Eulerian models.

Updating of the boundary conditions on the free-surface and on the radiation boundary is accomplished using the fourth order Runge-Kutta method. Besides the built-in computation error of the method and the truncation error, there are two other possible sources of errors. The first of these involves the time evolution of the free surface and the velocity potentials at the surface, and the potentials of the radiation boundary condition. All of these are updated concurrently although the parameters are dependent on each other. Hence, the concurrent marching scheme uses previous values of the other dependent parameters. The second source is due to the consecutive solution of the boundary value problem and the initial value problems. Because the velocity field

of a given time is obtained from the concurrent solution of the boundary value problem which uses the surface and radiation boundary conditions derived from the previous time step. All of these errors described here are tried to be kept at a minimum by selecting sufficiently small time steps. The so-called Courant-Friedrichs-Lewy condition is the most common convergence criteria necessary for wave propagation problems is satisfied in the models developed in this study.

Since the expected solution of the problem involves sinusoids which are smooth functions, the Runge-Kutta method can be used with a constant time step size. If this had not been the case, versions of the integrator which use variable time steps based on a preset error criterion would be required for the non-smooth functions resulting in increased computational time.

The solution of the problem is started by specifying initial conditions obtained from the analytical solution of the linear wave theory boundary value problem. The model is then run for several periods and the amplitude and phase errors are checked. It is also possible to start computations with an initial free surface coinciding with the mean water level. However, in this case the compatibility of the free surface configuration with the wave input on $\partial\Omega$ is achieved slowly. In order to avoid excessively long simulation times and since the wave input will always be well defined the specification of initial conditions using the known input wave is satisfied. The phase velocity used in the radiation boundary condition also belongs to the input wave. This may also have been calculated using the methodology in the previously referred study (Orlanski, 1976). This is not preferred because the phase velocity of the input wave is well defined.

3.2. The 2D Irrotational Linear Wave Propagation Problem

Here the full problem will be divided into two consecutive problems as the numerical approach suggests. The time dependent PDEs at the free surface and the radiation boundary condition constitutes the initial value problem and the governing equation and boundary conditions of Neumann and Dirichlet type constitutes the boundary

value problem. These two problems are solved consecutively in time supplying the necessary values to each other. Starting with initial values, the time dependent boundary conditions are updated to the next time step solving both the initial value problems at the free surface and radiation boundary condition. The known velocity profile at the influx section is also updated. This process is then followed by the solution of the boundary value problem using the updated boundary conditions. Boundary value problem solution is used to calculate the necessary values, most of the time velocities, for the initial value problems for the solution of the next time step. Using the previous chapter's coordinate system and origin on a domain Ω where boundaries are respectively identified as the surface, bottom, influx, radiation boundaries $\partial\Omega_s$, $\partial\Omega_b$, $\partial\Omega_i$, $\partial\Omega_r$, the initial value problem without the initial conditions is

$$\frac{\partial\phi}{\partial t} + g\eta = 0 \quad \text{on} \quad \partial\Omega_s \tag{3.1}$$

$$\frac{\partial\eta}{\partial t} - \frac{\partial\phi}{\partial z} = 0 \quad \text{on} \quad \partial\Omega_s \tag{3.2}$$

$$\frac{\partial\phi}{\partial t} + C\frac{\partial\phi}{\partial x} = 0 \quad \text{on} \quad \partial\Omega_r \tag{3.3}$$

and the boundary value problem at time t is

$$\nabla^2\phi = 0 \quad \text{in} \quad \Omega \tag{3.4}$$

$$\phi = \phi(\mathbf{x}_s, t) \quad \mathbf{x}_s \in \partial\Omega_s \tag{3.5}$$

$$\frac{\partial\phi}{\partial z} = 0 \quad \text{on} \quad \partial\Omega_b \tag{3.6}$$

$$\phi = \phi(\mathbf{x}_r, t) \quad \mathbf{x}_r \in \Omega_r \tag{3.7}$$

$$\frac{\partial\phi}{\partial x} = u(\mathbf{x}_i, t) \quad \mathbf{x}_i \in \Omega_i \tag{3.8}$$

$$\tag{3.9}$$

Compared to the original problem, the nonlinear terms of order $(ak)^2$ in the DFSBC and KFSBC given in Equations 3.1 and 3.2 are dropped. Also, in the boundary value problem Dirichlet type boundary conditions are used on the free surface and on the radiation boundary, and Neumann type boundary conditions are specified at the influx boundary and on the bottom boundary. Here the horizontal velocities at the influx

boundary are denoted by $u(\mathbf{x}_i, t)$

3.3. Numerical Formulation of the Linear Problem

In the formulations that follow, index notation is used wherever necessary for the sake of simplicity. Therefore coordinates are sometimes be labeled as 1 for the horizontal and 2 for the vertical instead of x and z. Although the numerical approach is approximate, the same parameter names will be used in the formulation. Accordingly the field parameter velocity potential can be expressed at the ith center located at $(x_i, z_i) \in \Omega \cup \partial\Omega$ in the form,

$$\phi_i = \Phi_{ij}\alpha_j \qquad i, j = 1, \ldots, N \tag{3.10}$$

α_j's are the coefficients of the interpolant, N is the number of centers taken. Φ_{ij} is the matrix with entries composed of MQs as shown below.

$$\Phi_{ij} = [(x_i - x_j)^2 + (z_i - z_j)^2 + c^2]^{1/2} \tag{3.11}$$

Once the coefficients are determined at the original centers, it is possible to find the derivatives at the locations of the centers easily. According to the definition in Equation 3.10 above, the velocity components, (u_i, w_i) and the Laplacian of the velocity potential at the ith center becomes,

$$u_i = \Phi_{ij,1}\alpha_j \tag{3.12}$$

$$w_i = \Phi_{ij,2}\alpha_j \tag{3.13}$$

$$\nabla^2\phi_i = \Phi_{ij,kk}\alpha_j \tag{3.14}$$

where $i, j = 1, \ldots, N$, $k = 1, 2$ and subscripts following the comma indicate the directions along which differentiation is performed. For the boundary value problem given by Equations 3.4 through 3.8 above, the asymmetrical system of equations can

be defined at instant t as

$$A_{ij}\alpha_j = b_i \tag{3.15}$$

where

$$A_{ij} = \begin{cases} \Phi_{ij} & (x_i, z_i) \in \partial\Omega_s \cup \partial\Omega_r \\ \Phi_{ij,1} & (x_i, z_i) \in \partial\Omega_i \\ \Phi_{ij,2} & (x_i, z_i) \in \partial\Omega_b \\ \Phi_{ij,kk} & (x_i, z_i) \in \Omega \end{cases} \tag{3.16}$$

and

$$b_i = \begin{cases} \phi(x_i, z_i, t) & (x_i, z_i) \in \partial\Omega_s \cup \partial\Omega_r \\ u(x_i, z_i) & (x_i, z_i) \in \partial\Omega_i \\ 0 & (x_i, z_i) \in \partial\Omega_b \cup \Omega \end{cases} \tag{3.17}$$

b_i is the component of time dependent right hand side vector. Using the definitions of ϕ given in Equation 3.10, one can construct the velocity potentials and the velocity components at the centers as shown below.

$$\phi_i = \Phi_{ij}\alpha_j = \Phi_{ij}A^{-1}_{jk}b_k \tag{3.18}$$

$$u_i = \Phi_{ij,1}\alpha_j = \Phi_{ij,1}A^{-1}_{jk}b_k \tag{3.19}$$

$$w_i = \Phi_{ij,2}\alpha_j = \Phi_{ij,2}A^{-1}_{jk}b_k \tag{3.20}$$

Here, A^{-1}_{ij} corresponds to an entry of the inverse of A_{ij}. As noted previously, the unsymmetrical system matrix A_{ij} and its inverse A^{-1}_{ij} as well as the interpolation matrix Φ_{ij} and its derivatives are set up once at the beginning of the computations so that their products are calculated once and in time, the only thing left is to fill in and update the entries of the right hand side vector. Multiplying appropriate matrices with the right hand side vector gives the approximate solution to the field unknowns. These unknowns are then used to determine the necessary input for the initial value

problems at the boundaries.

The time integration using the Runge-Kutta method can be formulated at a center i between two consecutive time steps differing by Δt as follows. For the free surface velocity potentials, free surface displacements and radiation boundary velocity potential

$$(k_1^{\phi_s})_i = -g\Delta t\,\eta_i \tag{3.21}$$
$$(k_1^{\eta})_i = \Delta t\,w_i \tag{3.22}$$
$$(k_1^{\phi_r})_i = -\Delta t\,u_i \tag{3.23}$$

whenever η_i, w_i and u_i are the values at time t. The time is then set to $t = t + 0.5\Delta t$, and

$$(k_2^{\phi_s})_i = -g\Delta t\,\eta_i \tag{3.24}$$
$$(k_2^{\eta})_i = \Delta t\,w_i \tag{3.25}$$
$$(k_2^{\phi_r})_i = -\Delta t\,u_i \tag{3.26}$$

whenever η_i, w_i and u_i are calculated after $\eta_i \leftarrow \eta_i + 0.5(k_1^{\eta})_i$, and $\phi_i \leftarrow \phi_i + 0.5(k_1^{\phi})_i$ both at the free surface and radiation boundary centers. In order to differentiate between the velocity potentials at the free surface and radiation boundary superscripts ϕ_s and ϕ_r are used. Again at time $t = t + 0.5\Delta t$,

$$(k_3^{\phi_s})_i = -g\Delta t\,\eta_i \tag{3.27}$$
$$(k_3^{\eta})_i = \Delta t\,w_i \tag{3.28}$$
$$(k_3^{\phi_r})_i = -\Delta t\,u_i \tag{3.29}$$

whenever η_i, w_i and u_i are calculated after $\eta_i \leftarrow \eta_i + 0.5(k_2^{\eta})_i$, and $\phi_i \leftarrow \phi_i + 0.5(k_2^{\phi})_i$ both at the free surface and radiation boundary centers. Finally, at time $t = t + \Delta t$

$$(k_4^{\phi_s})_i = -g\Delta t\,\eta_i \tag{3.30}$$

$$(k_4^{\eta})_i = \Delta t\, w_i \tag{3.31}$$

$$(k_4^{\phi_r})_i = -\Delta t\, u_i \tag{3.32}$$

whenever η_i, w_i and u_i are calculated after replacements such that $\eta_i \leftarrow \eta_i + (k_3^{\eta})_i$, and $\phi_i \leftarrow \phi_i + (k_3^{\phi})_i$ both at the free surface and radiation boundary centers. Hence, the updated values can be expressed as,

$$\phi_i|_{t+\Delta t} = \phi_i|_{\,t} + \frac{1}{6}\,(k_1^{\phi_s} + 2k_2^{\phi_s} + 2k_3^{\phi_s} + k_4^{\phi_s})_i \qquad (x_i, z_i) \in \partial\Omega_s \tag{3.33}$$

$$\eta_i|_{t+\Delta t} = \eta_i|_{\,t} + \frac{1}{6}\,(k_1^{\eta} + 2k_2^{\eta} + 2k_3^{\eta} + k_4^{\eta})_i \qquad (x_i, z_i) \in \partial\Omega_s \tag{3.34}$$

$$\phi_i|_{t+\Delta t} = \phi_i|_{\,t} + \frac{1}{6}\,(k_1^{\phi_r} + 2k_2^{\phi_r} + 2k_3^{\phi_r} + k_4^{\phi_r})_i \qquad (x_i, z_i) \in \partial\Omega_r \tag{3.35}$$

4. NONLINEAR WAVE PROPAGATION

In this part of the study, the full form of the boundary conditions as introduced in Chapter 2 is used without any simplifications. The model to be developed here, compared to the linear model, requires a free surface updating scheme since the small amplitude wave assumption is no longer used and as a consequence Taylor's expansions of the free surface boundary conditions about the mean water level are no longer possible.

The first model was developed so that the implementation of the full free surface boundary conditions and the free surface updating scheme could be facilitated without having to deal with a nonlinear input. Some error, on the order of $(ak)^2$, was accepted a priori since the nonlinear input wave can only satisfy the nonlinear free surface conditions up to order ak. A brief presentation of the results obtained using this model will be included.

With the experience gained from the first model, nonlinear wave input from the stream function wave theory was introduced in the development of the second model. The second model aims to show that even with a nonlinear wave input such as that from the stream function wave theory, the MQ based numerical method simulates wave propagation with sufficient accuracy.

Initially, the Sommerfeld radiation boundary condition was employed in both of these models and the phase velocity of the fundamental mode of the nonlinear wave was used in the computations. The Sommerfeld radiation boundary condition is known to work well with linear wave propagation normal to boundaries. Thus the utility of this boundary condition in the models developed was limited. The results were in good agreement with the initially assumed wave form for only a very limited time. As the simulation time increased, even the initially successful cases fail because of the nonlinearities allowed in the radiation boundary conditions. The nonlinear terms, even for the very small amplitude case, produce errors that develop in time so that

the Sommerfeld radiation boundary condition fails. Overall, the results obtained from the nonlinear stream function input model with the Sommerfeld boundary condition was not in good agreement with the assumed wave form. Therefore, the Sommerfeld radiation boundary condition was replaced with the periodic boundary condition and the solutions were generated over a domain of one wavelength in the horizontal.

As mentioned previously, the implementation of the nonlinear free surface boundary conditions necessitates the updating of the computational centers located on it. If the fully Lagrangian algorithm is used for this purpose, the updated locations of the surface centers are found directly using Equations 1.15 through 1.17. As the surface centers execute their motions, there is the chance that those centers closest to the vertical boundaries may leave the solution domain. This means that in order to be able to represent the free surface using a given number of centers, new ones need to be introduced. In addition, centers as they move may become very close to one another resulting in ill conditioned system matrices. To deal with these problems, the new locations of the free surface centers must be inspected every time step, new ones introduced as necessary and the locations of the problematic ones adjusted using interpolation. The technique adopted here was to adjust the new locations of all centers so that they coincide with their original horizontal locations.

On the other hand, as the semi-Lagrangian algorithm keeps track of the vertical displacements of the surface centers located at fixed horizontal positions, additional checking and adjusting of center locations at the free surface are avoided.

In the computations it is possible to use fixed or varying locations for centers within the solution domain. For the nonlinear model with linear input(NMLI), all centers inside the solution domain were placed and kept fixed well below the input wave trough level. This approach avoids the necessity of checking for centers that may be left outside the solution domain as the wave propagates. For the nonlinear model with nonlinear input(NMNI) following the determination of the free surface configuration through the application of the semi-Lagrangian algorithm, internal centers were redistributed over the depth from the bottom to the free surface. Thus, a fixed number of

centers were maintained at every vertical section.

4.1. Numerical Formulation

The numerical solution of the nonlinear wave propagation problem follows along the lines of that of linear wave propagation problem. That is, the solution of the boundary value problem and the initial value problems on the boundaries are interlaced. The set up of the system equations to be solved is

$$A_{ij}\alpha_j = b_i \qquad i,j = 1,\ldots,N \tag{4.1}$$

where the wave input(linear or nonlinear) is contained in the right hand side vector **b**. The system matrix A_{ij} is unsymmetrical as before. The solution of the system above is followed by the updating process. For the NMLI, entries of the system matrix dependent on the surface node locations are updated. When stream function wave theory input is used in the nonlinear model, updating at all the nodes except those on the bottom boundary is required.

Whereas the solution of the linear wave problem involved a single matrix inversion followed by matrix vector multiplications as time progressed, the updating process involved in the solution of the nonlinear wave propagation problem necessitates matrix inversion each time step. Since matrix inversion is a costly process, both in terms of time and computer resources and particularly as the size of the system matrix increases, the overall cost of running the nonlinear model can be relatively high for large-scale problems or extended simulation times.

Once the velocity potentials are determined from the boundary value problem, initial value problems are solved to determine the positions of the surface at the next time step and the velocity potentials both the free surface and the radiation boundary to be used as Dirichlet type boundary conditions for the solution of the potentials of the next time step throughout the domain.

The free surface boundary conditions for the fully Lagrangian approach are,

$$\frac{Dx_L}{Dt} = u_L \tag{4.2}$$
$$\frac{Dz_L}{Dt} = w_L \tag{4.3}$$
$$\frac{D\phi_L}{Dt} = \frac{1}{2}\left|\boldsymbol{\nabla}\phi_L\right|^2 - gz_L \tag{4.4}$$

Their corresponding time discretizations, between the time steps at times t and $t+\Delta t$, are

$$(x_L)_i|_{t+\Delta t} = (x_L)_i|_{t+\Delta t} + \frac{1}{6}\left(k_1^{x_L} + 2k_2^{x_L} + 2k_3^{x_L} + k_4^{x_L}\right)_i \qquad (x_i, z_i) \in \partial\Omega_s \tag{4.5}$$
$$(z_L)_i|_{t+\Delta t} = (z_L)_i|_{t+\Delta t} + \frac{1}{6}\left(k_1^{z_L} + 2k_2^{z_L} + 2k_3^{z_L} + k_4^{z_L}\right)_i \qquad (x_i, z_i) \in \partial\Omega_s \tag{4.6}$$
$$(\phi_L)_i|_{t+\Delta t} = (\phi_L)_i|_{t+\Delta t} + \frac{1}{6}\left(k_1^{\phi_L} + 2k_2^{\phi_L} + 2k_3^{\phi_L} + k_4^{\phi_L}\right)_i \qquad (x_i, z_i) \in \partial\Omega_s \tag{4.7}$$

One important point that has to be noted is that while the equations above use Lagrangian coordinates, the identification of where the ith center located is made using the coincident Eulerian frame. The main connection between the time discretization with respect to Eulerian coordinate system and Lagrangian coordinate system is realized considering that the particles are the centers for one moment and the Lagrangian positions at a later time gives the positions of the centers over which the Eulerian surface passes.

The initial value problem on the radiation boundary remains the same in all of the models (see Equation 3.3),therefore its numerical formulation is omitted here to avoid repetition. The computation of the free surface k_1s at the ends and middle of a time step during the computation are as follows.

$$(k_1^{x_L})_i = \Delta t\,(u_L)_i \tag{4.8}$$
$$(k_1^{z_L})_i = \Delta t\,(w_L)_i \tag{4.9}$$
$$(k_1^{\phi_L})_i = \frac{1}{2}\Delta t\,\left|\boldsymbol{\nabla}(\phi_L)_i\right|^2 - g\Delta t\,(z_L)_i \tag{4.10}$$

whenever u_L, w_L, ϕ_L and z_L belong to time t. There are two important steps before passing to the evaluation of k_2s. First, the positions and potentials of the centers are updated via the assignments $x_L \leftarrow x_L + 0.5k_1^{x_L}$, $z_L \leftarrow z_L + 0.5k_1^{z_L}$, $\phi_L \leftarrow \phi_L + 0.5k_1^{\phi_L}$. Second, using these values, the boundary value problem is solved to get the velocities at the interpolated centers as the algorithm suggests. The interpolation is performed in two steps. In the first step, elevations which are a function of the horizontal positions at an instant are interpolated at the fixed coordinates x_L^fs using the updated values, namely x_Ls and z_L. Given the set of points x_L, z_L at the free surface, the coefficients of the interpolant for the elevations are computed by,

$$\alpha_i = \Phi_{ij}^{-1}(z_L)_j \tag{4.11}$$

where

$$\Phi_{ij} = [((x_L)_i - (x_L)_j)^2 + c^2]^{1/2} \tag{4.12}$$

Then the elevations $(z_L^f)_i$s of the horizontally fixed centers at $(x_L^f)_i$s are

$$(z_L^f)_i = [((x_L^f)_i - (x_L)_j)^2 + c^2]^{1/2}\alpha_j \tag{4.13}$$

where x_Ls are updated coordinates used in the interpolant Equation 4.12 above and α_js are the coefficients evaluated by Equation 4.11. In the second step, velocity potentials of these interpolated centers are obtained by interpolation using the updated positions (x_L, z_L)s and the corresponding potentials ϕ_Ls. The potentials are interpolated in a similar manner, but this time the interpolation is performed in two dimensions because the potentials at an instant are a function of the horizontal and vertical coordinates. Hence the interpolation coeffients become,

$$\alpha_i = \Phi_{ij}^{-1}(\phi_L)_j \tag{4.14}$$

where

$$\Phi_{ij} = [((x_L)_i - (x_L)_j)^2 + ((z_L)_i - (z_L)_j)^2 + c^2]^{1/2} \tag{4.15}$$

Then the potentials, $(\phi_L^f)_i$s, of the horizontally fixed centers at $((x_L^f)_i, (z_L^f)_i)$s are

$$(\phi_L^f)_i = [((x_L^f)_i - (x_L)_j)^2 + ((z_L^f)_i - (z_L)_j)^2 + c^2]^{1/2}\alpha_j \tag{4.16}$$

At this point, the boundary value problem is solved to get velocity components u_L and w_Ls and calculations at the mid-time step $t \leftarrow t + 0.5\Delta\, t$. The k_2s may be given as

$$(k_2^{x_L})_i = \Delta t\,(u_L)_i \tag{4.17}$$

$$(k_2^{z_L})_i = \Delta t\,(w_L)_i \tag{4.18}$$

$$(k_2^{\phi_L})_i = \frac{1}{2}\Delta t\ |\boldsymbol{\nabla}(\phi_L)_i|^2 - g\Delta t\,(z_L)_i \tag{4.19}$$

where z_L and ϕ_L are used instead of z_L^f and ϕ_L^f

Next, the k_3s are evaluated after updating the positions and the potentials of the previous time step by half of the k_2s found above and interpolating the necessary values at locations fixed in the horizontal. If the positions and potentials of the previous time step are denoted by x_L,z_L and ϕ_L, the updated positions and potentials can be denoted by $x_L + 0.5k_2^{x_L}$, $z_L + 0.5k_2^{z_L}$ and $\phi_L + 0.5k_2^{\phi_L}$. This is followed by the interpolation process of the positions and potentials to fixed locations along the horizontal in a similar manner as described above before the calculation of the k_2s. Hence,

$$(k_3^{x_L})_i = \Delta t\,(u_L)_i \tag{4.20}$$

$$(k_3^{z_L})_i = \Delta t\,(w_L)_i \tag{4.21}$$

$$(k_3^{\phi_L})_i = \frac{1}{2}\Delta t\ |\boldsymbol{\nabla}(\phi_L)_i|^2 - g\Delta t\,(z_L)_i \tag{4.22}$$

where z_L^f and ϕ_L^f are replaced by z_L and ϕ_L.

Finally k_4s given below are evaluated at the end of the time step with the assignment $t \leftarrow t + \Delta\, t$.

$$(k_4^{x_L})_i = \Delta t\,(u_L)_i \tag{4.23}$$

$$(k_4^{z_L})_i = \Delta t\,(w_L)_i \tag{4.24}$$

$$(k_4^{\phi_L})_i = \frac{1}{2}\,\Delta t\;|\boldsymbol{\nabla}\phi_L|^2 - g\Delta t\, z_L \tag{4.25}$$

where u_L and w_L are derived from the potentials obtained from the solution of boundary value problem in which the positions and potentials of the surface centers are found by the interpolation to the fixed locations along the horizontal of the updated positions and potentials. The positions and potentials of the previous time step that can be denoted by x_L,z_L and ϕ_L after updating will become $x_L + k_3^{x_L}$, $z_L + k_3^{z_L}$ and $\phi_L + k_3^{\phi_L}$.

On the other hand, NMNI uses the full form of the originally introduced Eulerian KFSBC in Equation 2.3, whereas the DFSBC is modified so that only vertical displacements of the surface particles are kept track of. Here only the time discretizations of the free surface boundary conditions are given. Recalling the free surface boundary conditions,

$$\frac{\partial\phi_s}{\partial t} = -g\eta - \frac{1}{2}\mid\boldsymbol{\nabla}\phi\mid^2 + \frac{\partial\phi}{\partial z}\frac{\partial\eta}{\partial t} \tag{4.26}$$

$$\frac{\partial\eta}{\partial t} = -\frac{\partial\phi}{\partial x}\frac{\partial\eta}{\partial x} + \frac{\partial\phi}{\partial z} \tag{4.27}$$

their time marching scheme between time steps t and $t+\Delta t$ will be expressed as follows.

$$(k_1^{\phi})_i = \Delta t\Big[-g\eta_i - \frac{1}{2}\,|\boldsymbol{\nabla}\phi_i|^2 + w_i\eta_{i,t}\Big] \tag{4.28}$$

$$(k_1^{\eta})_i = \Delta t\Big[-u_i\eta_{i,x} + w_i\Big] \tag{4.29}$$

All the necessary values, η_i, ϕ_i, w_i, $\eta_{i,t}$, u_i and $\eta_{i,x}$, belong to time level t. The

next set at time $t \leftarrow t + 0.5\Delta t$ is calculated after the computation of w_i, $\eta_{i,t}$, u_i and $\eta_{i,x}$ where the surface centers at fixed horizontal positions are carried to their new elevations $\eta_i \leftarrow \eta_i + 0.5(k_1^\eta)_i$ with their newly updated potentials $\phi_i \leftarrow \phi_i + 0.5(k_1^\phi)_i$. These updated potentials are used as an input to the boundary value problem besides some other necessary input such as the potentials of the radiation boundary. Therefore,

$$(k_2^\phi)_i = \Delta t\Big[- g\eta_i - \frac{1}{2}\left|\boldsymbol{\nabla}\phi_i\right|^2 + w_i\eta_{i,t}\Big] \tag{4.30}$$

$$(k_2^\eta)_i = \Delta t\Big[- u_i\eta_{i,x} + w_i\Big] \tag{4.31}$$

The surface centers at fixed positions are carried to their new elevations $\eta_i \leftarrow \eta_i + 0.5(k_2^\eta)_i$ with their newly updated potentials $\phi_i \leftarrow \phi_i + 0.5(k_2^\phi)_i$. Similar to the previous step but without updating the time, the k_3s are evaluated after the determination of w_i, $\eta_{i,t}$, u_i and $\eta_{i,x}$ solving the boundary value problem before. Hence,

$$(k_3^\phi)_i = \Delta t\Big[- g\eta_i - \frac{1}{2}\left|\boldsymbol{\nabla}\phi_i\right|^2 + w_i\eta_{i,t}\Big] \tag{4.32}$$

$$(k_3^\eta)_i = \Delta t\Big[- u_i\eta_{i,x} + w_i\Big] \tag{4.33}$$

Finally, the time is updated to $t \leftarrow t + \Delta t$. The surface centers are carried to their new elevations $\eta_i \leftarrow \eta_i + (k_3^\eta)_i$ with their newly updated potentials $\phi_i \leftarrow \phi_i + (k_3^\phi)_i$ and used as an input to the boundary value problem which is followed by the computation of w_i, $\eta_{i,t}$, u_i and $\eta_{i,x}$ for the k_4s as expressed below.

$$(k_4^\phi)_i = \Delta t\Big[- g\eta_i - \frac{1}{2}\left|\boldsymbol{\nabla}\phi_i\right|^2 + w_i\eta_{i,t}\Big] \tag{4.34}$$

$$(k_4^\eta)_i = \Delta t\Big[- u_i\eta_{i,x} + w_i\Big] \tag{4.35}$$

Using all these k_is, time discretizations of the velocity potential and the free

surface displacements are given below.

$$\phi_i|_{t+\Delta t} = \phi_i|_t + \frac{1}{6}\,(k_1^\phi + 2k_2^\phi + 2k_3^\phi + k_4^\phi)_i \tag{4.36}$$

$$\eta_i|_{t+\Delta t} = \eta_i|_t + \frac{1}{6}\,(k_1^\eta + 2k_2^\eta + 2k_3^\eta + k_4^\eta)_i \tag{4.37}$$

5. NUMERICAL TESTS and RESULTS

In this chapter, the results of some selected numerical tests are given and compared with the known solution in terms of the free surface displacements. Besides targeting a free surface conforming to the known surface, it is also aims to show the effects of various parameters affecting the solutions. There are several parameters involved in the problem. These are input wave dependent ones such as wave steepness, problem dimensions such as the length, height of the domain, computationally necessary parameters such as the time step and the shape parameter of the MQ function.

Since we are dealing with wave propagation, the well established Courant-Friedrichs-Lewy (CFL)condition linking the spatial and temporal step sizes must be adhered to. As the models developed here involve centers which move in time, the varying ratio of the spatial to temporal step size may violate the CFL condition during program execution. To avoid any such violation, a small time step of one-hundredth of a second was chosen and found to work well. Naturally, each case that was run has a longest possible time step, but no attempt was made to determine its value. Time steps of smaller that one-hundredth of a second were tried and found not to contribute toward increasing accuracy of the results.

Wave steepness is the most critical parameter in the construction of the numerical solution. As long as the steepness criterion of the linear model is satisfied, wave steepness has no effect on the accuracy of the results. On the other hand, in the nonlinear models, parallel to the well known fact that the steeper the wave, the steeper the wave, the harder it is to obtain accurate results, the numerical tests performed in this study have shown that beyond a limiting steepness the accuracy of the results deteriorates. One of the important reasons for the loss in accuracy may be attributed to the constant shape parameter, c, used. As c depends on the distribution of centers within the solution domain, the constant value chosen at the beginning of the simulation actually needs to be modified as the centers move.

Given a wave, resolution of the centers is another important factor in obtaining accurate results. Centers very sparsely distributed throughout the domain may not suffice to provide accurate solutions. In all of the three models a certain number of points along the horizontal and the vertical are placed during the computation. Since the linear model uses all the time fixed centers, a regular grid is formed over the rectangular solution domain. It has been experienced that the steeper waves demanded higher resolution than those required by the less steep waves. On the other hand, too high resolutions not only result in unacceptably long computation times but also lead ill-conditioned system matrices and to non-converging schemes.

Once the adequate resolution is maintained for a given wave, one other adjustment necessary to obtain accurate solution is on the shape parameter. Despite the fact that there are some studies that suggest values of the shape parameter (Wu and Hon, 2003), there is no general agreement as to the optimum value of c^2. In particular, none of these studies was done for a case where a moving boundary and moving centers were present. Therefore, the strategy adopted here was to use the suggested c^2's as rough indicators of where to hunt for the optimum c^2 and then to refine this value by trial and error. It has been determined that if the spacings between the consecutive centers in the vertical range from 0.25 m to 0.5 m and the spacings in the horizontal are 1.5 times of the vertical spacing, the optimum squared shape parameter ranges from 2 to 12. This observation strengthens the fact that the selection of a constant shape parameter in the simulation affects the accuracy of the interpolation. Because given a wavelength increasing the wave height to increase the steepness affects the aspect ratio of vertical to horizontal consecutive center spacings as the vertical spacings below the trough are different from those below the crest while the horizontal spacing is uniform throughout the domain.

The tests are performed using desktop computers with Pentium IV processors operating at internal speeds of 3.0 GHz and 2.6 GHz. The physical memories of the desktops were sufficient to store the variables and matrices so virtual memory is not used during the simulations performed in this study. Therefore the difference between the internal speeds is not important to require desktop computer specific classification

of the tests.

5.1. Linear Model Results

Twenty-one different numerical tests are selected to show the performance of the linear model and summarized in Table 5.1 to Table 5.3. The results in Table 5.1 correspond to a shallow water wave and Table 5.2 to a deep water wave and Table 5.3 to an intermediate water wave. Here, besides the wave parameters H, L, T, H/L and depth d, the horizontal length of the domain, W, the number of centers along the horizontal and vertical, nx, nz, consecutive center spacings along the horizontal and vertical dx, dz, the square of the MQRBF shape parameter, c^2, the run-rime, R.T., maximum percentage relative error in terms of wave height $\epsilon\%$ at the instant nT where nT is the actual computation duration are also given. The simulation times of these tests range from 4 seconds to 357 seconds. The horizontal length of the solution domain was selected as one wave length so that the Sommerfeld radiation condition and the periodic boundary conditions would be employed interchangeably for any given test case. The computation centers were placed so that the ratio of the horizontal to vertical spacing was 1.5. The last column is the number of periods after which computation is stopped and at which the maximum relative errors are calculated in terms of the wave height.

As a demonstration of how the optimum shape parameter was determined, Figure 5.1, showing the variation of maximum relative errors in the first eight tests with respect to c^2, is given. After 8 trials, $c^2 = 12$ was found to be the optimum value for the configuration of the tests given in detail in Table 5.1. Figure 5.1 shows that beyond the optimum $c^2 = 12$, the relative error increases sharply. From personal experience reported in studies such as those by Wu and Hon (2003), Hon et al. (1999), it is known that errors will continue to increase beyond the optimum point and finally the system matrix will become singular as c^2 dominates the RBF. The resulting free surfaces of the best and the worst of these 8 test cases as well as the assumed profile are plotted in the Figure 5.2. Also, phase errors, besides the computed relative amplitude errors at the given instants could have been given but they are negligibly small as seen in the

figure.

As summarized in Table 5.1, tests T09 to T15 share the same maximum relative error while their steepness values change. Starting from a steepness of 0.0071, the same accuracy is obtained up to 0.14 with test T15. Although the waves become steeper, the results are almost not affected for the linear model. For the same purpose, tests T19 to T21 given in the Table 5.3 can also be noted where simulations are performed up to 20 periods.

On the other hand, the tests T16 to T19 are given to show that even the calculations are performed at various instants, the accuracy of the models cannot be distinguished. To illustrate this observation, Figure 5.3 is given.

Table 5.1. Summary of some selected linear model tests performed with a shallow water wave

ID	H[m]	L[m]	T[s]	H/L	d[m]	W[m]	nx	nz	dx	dz	c^2	$\epsilon\%$	ϵ_{rms}[mm]	R.T.[s]	nT
T01	0.1	103.5	15	0.001	5	103.5	141	11	0.74	0.50	7.000	2.56	1.3	357	5
T02	0.1	103.5	15	0.001	5	103.5	141	11	0.74	0.50	6.000	3.54	1.7	357	5
T03	0.1	103.5	15	0.001	5	103.5	141	11	0.74	0.50	8.000	1.86	0.9	357	5
T04	0.1	103.5	15	0.001	5	103.5	141	11	0.74	0.50	9.000	1.39	0.7	357	5
T05	0.1	103.5	15	0.001	5	103.5	141	11	0.74	0.50	10.000	1.06	0.5	357	5
T06	0.1	103.5	15	0.001	5	103.5	141	11	0.74	0.50	11.000	0.81	0.4	358	5
T07	0.1	103.5	15	0.001	5	103.5	141	11	0.74	0.50	12.000	0.6	0.3	357	5
T08	0.1	103.5	15	0.001	5	103.5	141	11	0.74	0.50	14.000	2.63	1.7	357	5

Table 5.2. Summary of some selected linear model tests performed with a deep water wave

ID	H[m]	L[m]	T[s]	H/L	d[m]	W[m]	nx	nz	dx	dz	c^2	$\epsilon\%$	ϵ_{rms}[mm]	R.T.[s]	nT
T09	0.1	14	3	0.0071	10	15	38	41	0.41	0.25	3.000	0.94	0.6	213	5
T10	0.2	14	3	0.0142	10	15	38	41	0.41	0.25	3.000	0.94	1.2	303	5
T11	0.3	14	3	0.0214	10	15	38	41	0.41	0.25	3.000	0.94	1.8	361	5
T12	0.4	14	3	0.0285	10	15	38	41	0.41	0.25	3.000	0.94	2.3	353	5
T13	0.5	14	3	0.0356	10	15	38	41	0.41	0.25	3.000	0.94	2.9	250	5
T14	1	14	3	0.0712	10	15	38	41	0.41	0.25	3.000	0.94	5.8	260	5
T15	2	14	3	0.1424	10	15	38	41	0.41	0.25	3.000	0.94	1.2	323	5

Table 5.3. Summary of some selected linear model tests performed with an intermediate water wave

ID	H[m]	L[m]	T[s]	H/L	d[m]	W[m]	nx	nz	dx	dz	c^2	$\epsilon\%$	ϵ_{rms}[mm]	R.T.[s]	nT
T16	0.1	30.3	5	0.0033	5	30.4	41	11	0.76	0.50	12.000	1.16	0.6	4	1
T17	0.1	30.3	5	0.0033	5	30.4	41	11	0.76	0.50	12.000	0.73	0.5	6	2
T18	0.1	30.3	5	0.0033	5	30.4	41	11	0.76	0.50	12.000	0.7	0.4	18	10
T19	0.1	30.3	5	0.0033	5	30.4	41	11	0.76	0.50	12.000	0.72	0.4	34	20
T20	0.2	30.3	5	0.0066	5	30.4	41	11	0.76	0.50	12.000	0.72	0.8	35	20
T21	0.4	30.3	5	0.0132	5	30.4	41	11	0.76	0.50	12.000	0.72	1.6	34	20

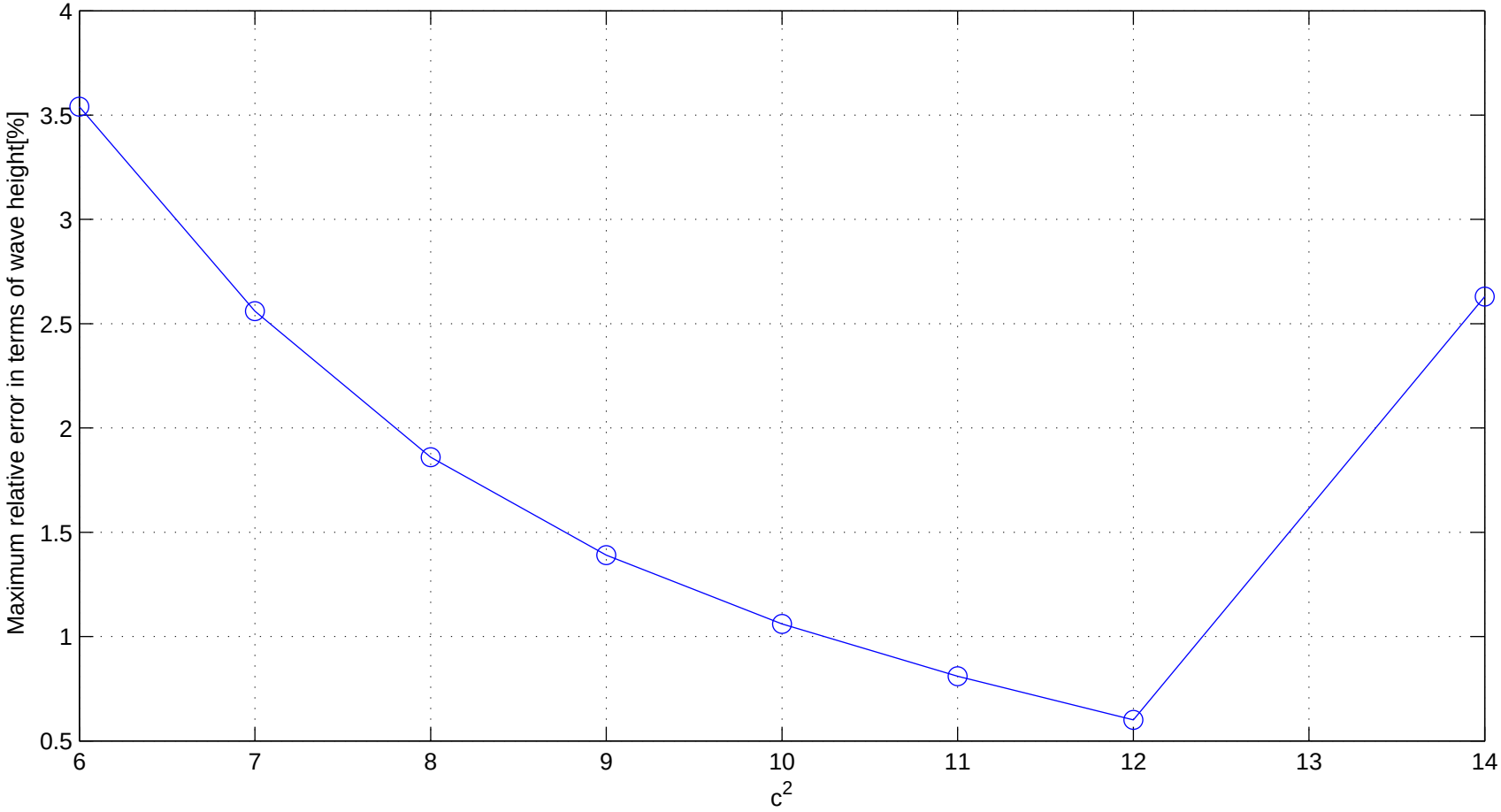

Figure 5.1. Variation of maximum relative error with respect to the shape parameter squared nT.(Tests T01 to T08 listed in Table 5.1)

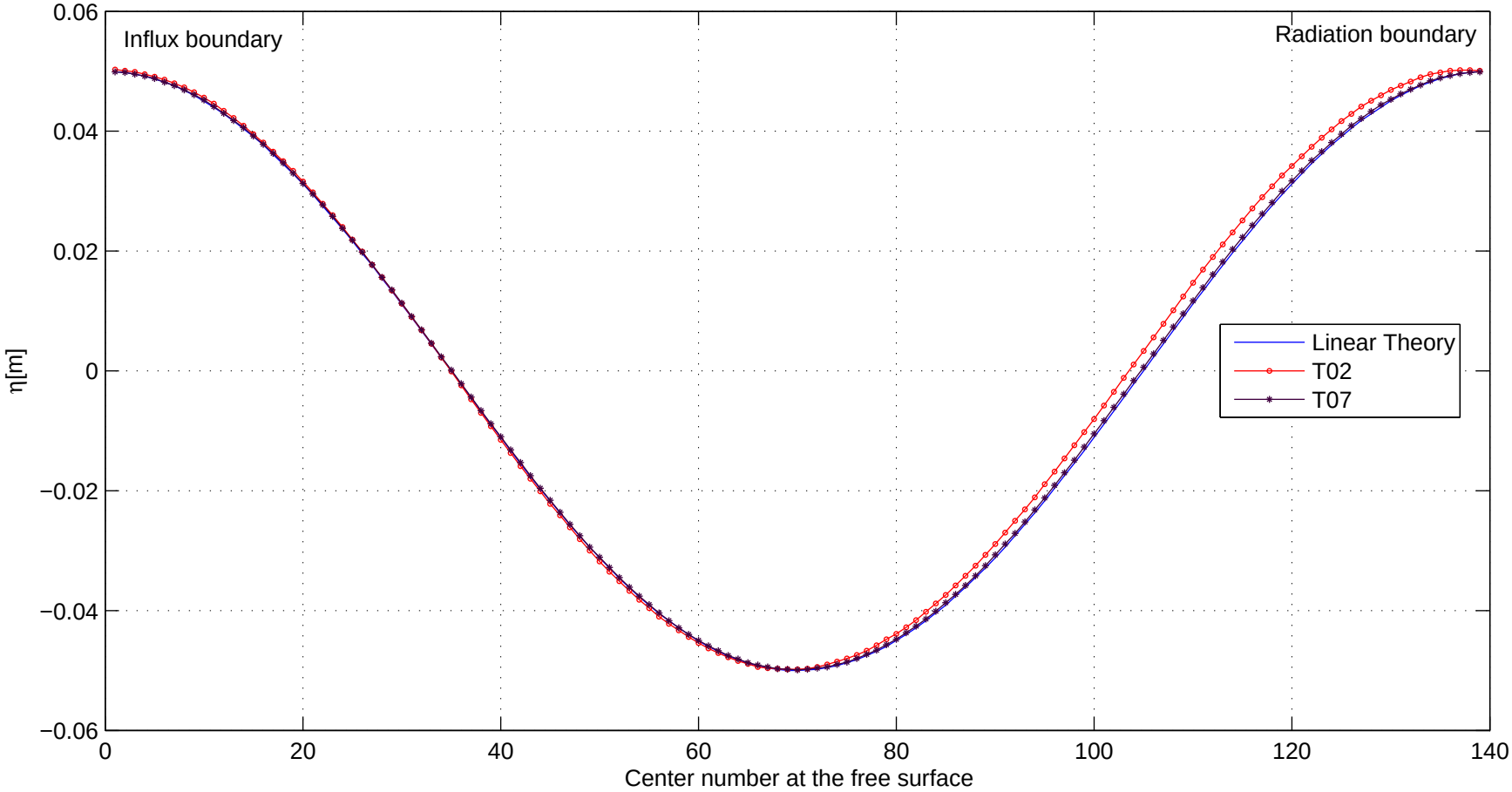

Figure 5.2. Variation of the free surface in shallow water

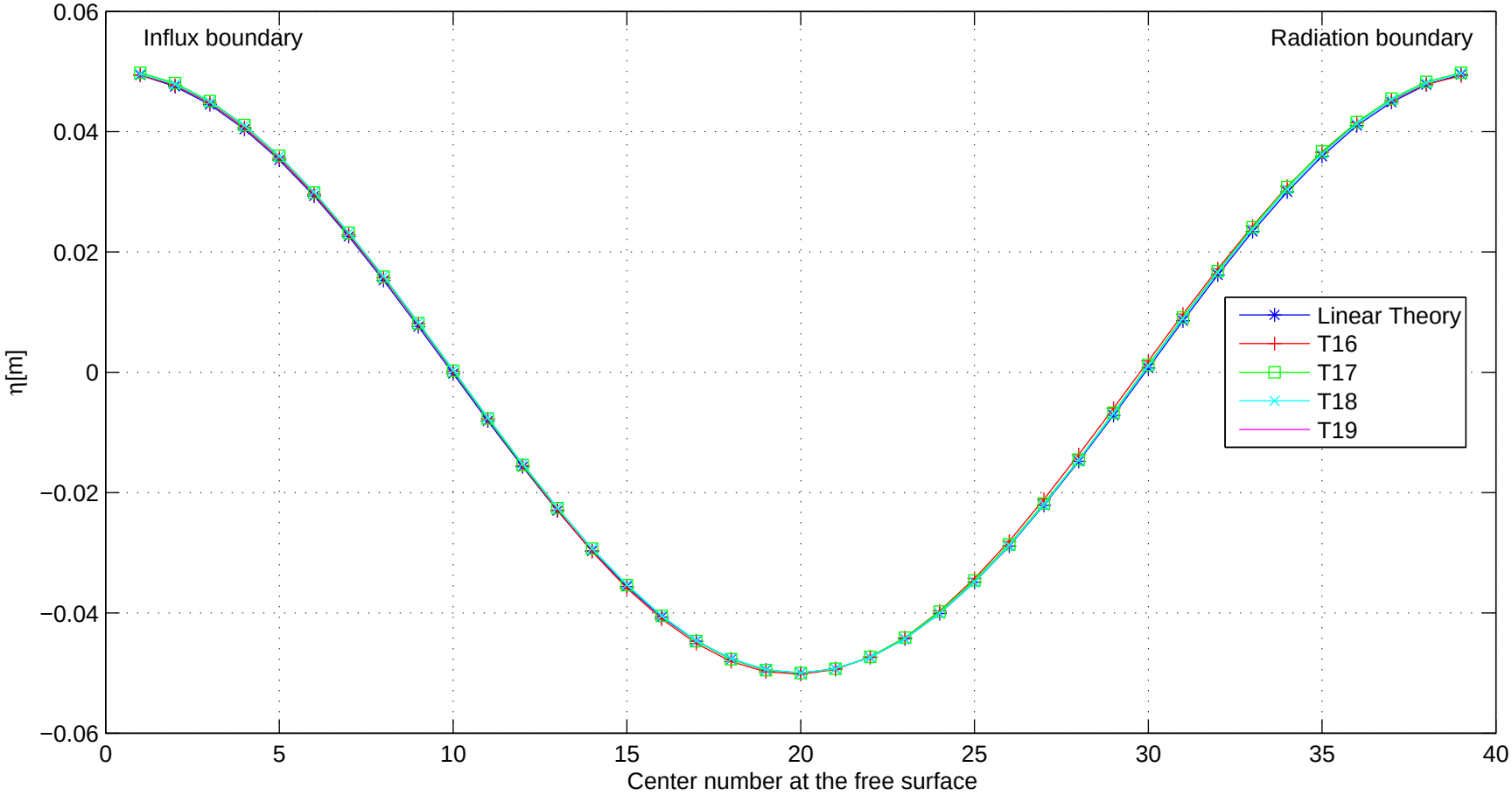

Figure 5.3. Variation of the free surface in intermediate water

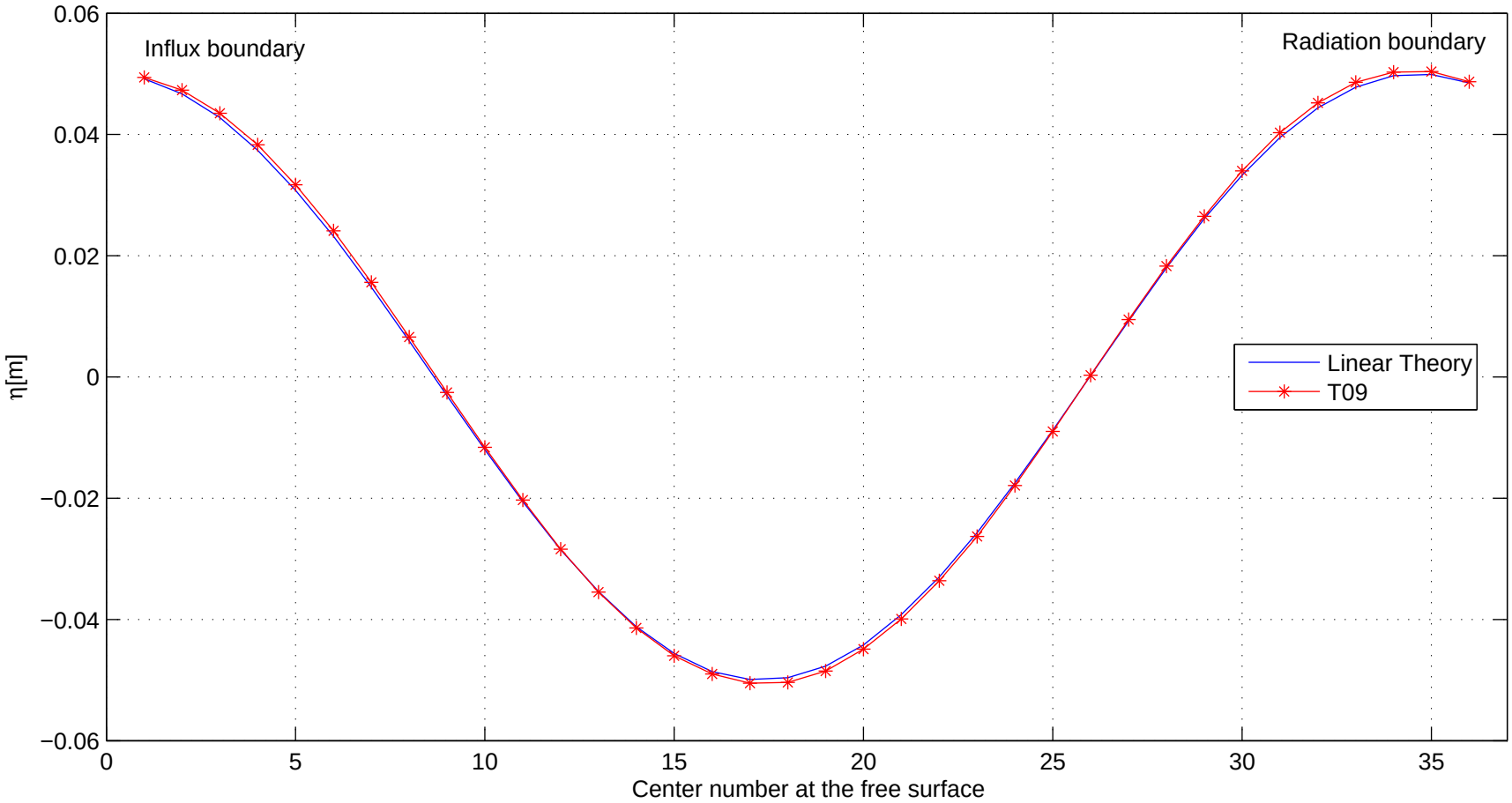

Figure 5.4. Variation of the free surface in deep water

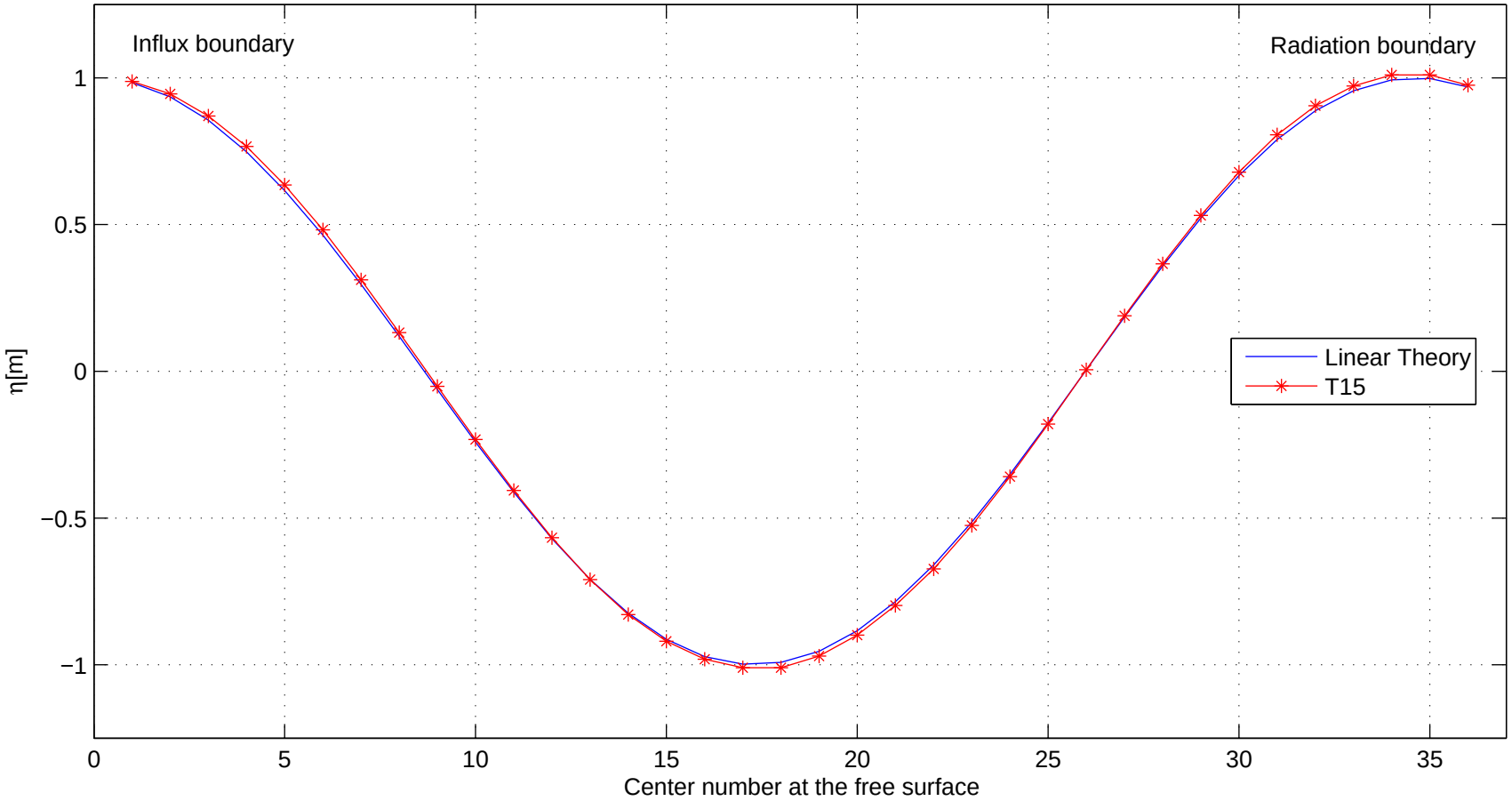

Figure 5.5. Variation of the free surface in deep water

5.2. Nonlinear Model with Linear Input Results

Initially this model was developed with the Sommerfeld radiation boundary condition. After several tests with this version of the model, it was observed that the accuracy of the results decreased considerably in time. Neither an increase in resolution, nor the adjustments to the MQ via the shape parameter helped to control the errors that developed in time. On the other hand, errors become unbounded in NMNI earlier than in the NMLI. These observations lead to the conclusion that the Sommerfeld radiation boundary condition fails to work well as long as nonlinear free surface boundary conditions are introduced into the model even though a linear wave input is used. This behavior can be attributed to the nature of the Sommerfeld radiation boundary condition which is known to admit only the fundamental mode of a wave. Table 5.4 summarizes the results of three tests performed using the Sommerfeld radiation boundary condition. Maximum relative error, which is 1.8% after one period the simulation has started, increased to 16.7% in three periods of run time and to very high levels in five periods of run time. These errors developed despite the fact that the input wave had a rather low steepness of 0.0031. The tests of Table 5.4 are plotted in Figure 5.6.

As a remedy, the Sommerfeld radiation boundary condition was replaced by a periodic boundary condition where the input wave data was duplicated at a distance of one wavelength. The wave input used was identical to the one given above. The results of the runs made are summarized in Table 5.5, and plotted in Figure 5.7. These results indicate noticeable improvement whereas the errors tended to increase and become unbounded in the previous case, here the errors are bounded and below 3% for a run over 6 wave periods.

Further testing of the NMLI model was discontinued as it was thought that it served its purpose of providing insight for the fully nonlinear model NMNI. The improvement in the accuracy of the results by replacing the Sommerfeld RBC with the periodic boundary condition in the model NMLI may seem to be due to the change in the number of centers and the optimum c^2 but replacing the input wave with a

steeper wave showed that accurate results are still obtained when the periodic boundary condition is used whereas the model with the Sommerfeld RBC could not produce reliable results.

Table 5.4. Summary of some selected NMLI tests with the Sommerfeld radiation boundary condition

ID	H[m]	L[m]	T[s]	H/L	d[m]	W[m]	nx	nz	dx	dz	c^2	$\epsilon\%$	ϵ_{rms}[mm]	R.T.[s]	nT
T22	0.1	32.2	5	0.0031	6	60.0	41	7	1.5	1	85	1.79	0.9	142	1
T23	0.1	32.2	5	0.0031	6	60.0	41	7	1.5	1	85	8.33	2.8	142	2
T24	0.1	32.2	5	0.0031	6	60.0	41	7	1.5	1	85	16.73	3.7	142	3
T25	0.1	32.2	5	0.0031	6	60.0	41	7	1.5	1	85	7.42	3.0	528	4
T26	0.1	32.2	5	0.0031	6	60.0	41	7	1.5	1	85	>100	>100	660	5

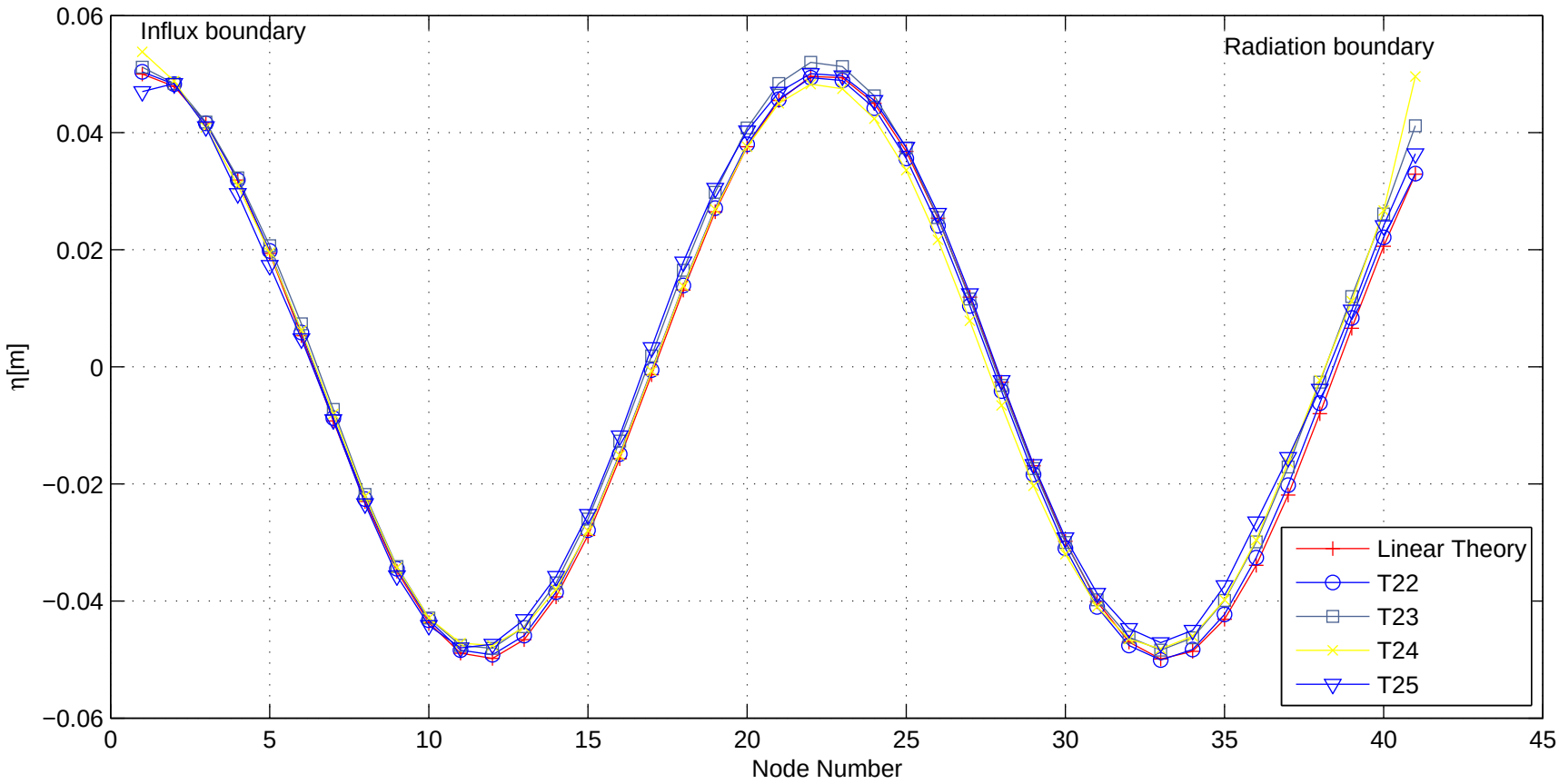

Figure 5.6. Free surface variation obtained from NMLI with the Sommerfeld RBC

Table 5.5. Summary of some selected NMLI tests with the periodic boundary condition

ID	H[m]	L[m]	T[s]	H/L	d[m]	W[m]	nx	nz	dx	dz	c^2	$\epsilon\%$	ϵ_{rms}[mm]	R.T.[s]	nT
T27	0.1	32.2	5	0.0031	6	32.2	20	16	1.7	0.4	10	2.5	1.7	216	1
T28	0.1	32.2	5	0.0031	6	32.2	20	16	1.7	0.4	10	1.8	1.0	858	4
T29	0.1	32.2	5	0.0031	6	32.2	20	16	1.7	0.4	10	2.7	1.6	1072	5
T30	0.1	32.2	5	0.0031	6	32.2	20	16	1.7	0.4	10	2.3	1.0	1286	6

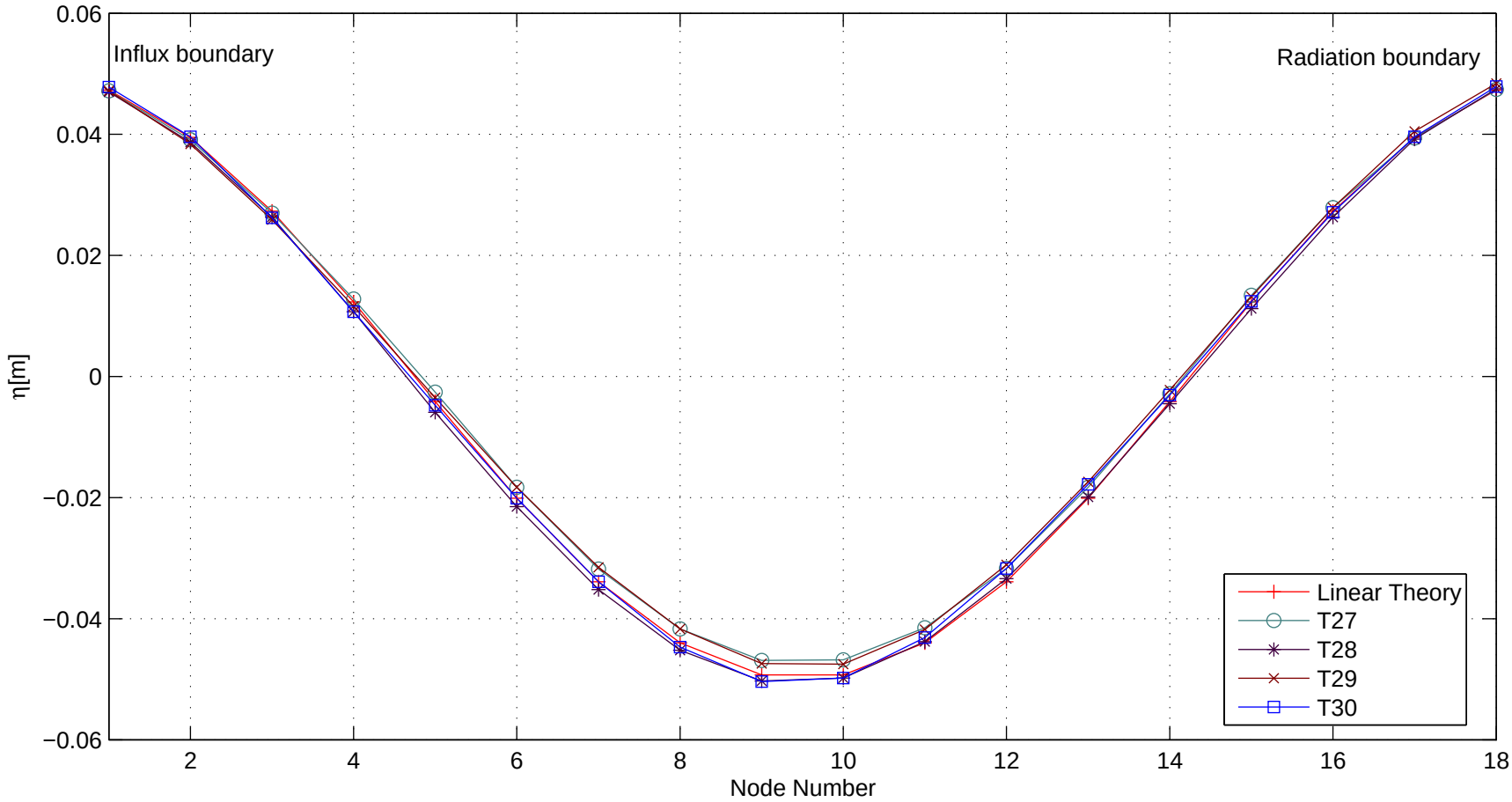

Figure 5.7. Free surface variation obtained from the NMLI with periodic boundary condition

5.3. Nonlinear Model with Nonlinear Input Results

For the implementation of the nonlinear model, the stream function wave theory was chosen to provide the wave input. The reason for the choice is that the stream function wave theory provides a best fit to the dynamic free surface boundary condition for all relative depths whereas for theories like Stokes V or Cnoidal I there are zones of validity (Dean and Dalrymple, 1984). The formulation of the stream function theory by Fenton (1988) was chosen as it allows the most straightforward computer implementation.

Although the MNLI runs indicated the inadequacy of the Sommerfeld RBC a single run was made using it to confirm the conclusion. All test reported here have been carried out using the periodic boundary condition.

Two waves approaching breaking in intermediate water were selected. Based on their primary modes, the first wave is in relatively deeper water, $d/L = 0.186$, and is less steep, $H/L = 0.078$. For the second wave $d/L = 0.094$ and $H/L = 0.0119$. Accordingly the two waves are represented by second and fourth order stream functions.

Table 5.6 corresponds to the tests of a second order stream function wave. The input wave with a wave height of 0.25 meters have its crest at 0.13 meters above and its trough level 0.12 meters below the mean water level. Tests T31 and T32 are run with the mesh constructed using 44 nodes along the horizontal and 12 nodes along the vertical. The maximum relative error is about 1% of the wave height and each period of simulation took about 15 minutes. The effect of using a coarser mesh to reduce the run time was investigated. Instead of the 528 centers used previously a new mesh consisting of 158 centers (22 in the horizontal by 7 in the vertical) was tried. The error, even at 8 periods of simulation was under 2%. Thus it can be seen that at a cost of 1% in the error the run time for one period is reduced from 885 seconds to 46 seconds. The test results are summarized in Table 5.6 and plotted in Figure 5.8 for tests T31 and T32, and in Figure 5.9 for tests T33 to T35.

The results given in the Table 5.7 corresponds to a fourth order stream function wave. This time the crest level is 0.15 meters above and the trough level is 0.1 meters below the mean water level for this wave of 0.25 meters in height. In all of the tests, maximum relative error in terms of wave height is around half of a percent even even after a simulation of 5 periods. The results are in perfect agreement with the input wave profile. The simulation of a single period took about 13 minutes using 448 centers. Variation of root mean square error corresponding to test T38 is also plotted in Figure 5.11.

Table 5.6. NMNI tests of a second order stream function wave

ID	Order	H[m]	L[m]	T[s]	H/L	d[m]	W[m]	nx	nz	dx	dz	c^2	$\epsilon\%$	ϵ_{rms}[mm]	R.T.[s]	nT
T31	2	0.25	32.2	5	0.0078	6	32.2	44	12	0.7	0.5	15	0.63	0.8	885	1
T32	2	0.25	32.2	5	0.0078	6	32.2	44	12	0.7	0.5	15	0.97	1.2	4585	5
T33	2	0.25	32.2	5	0.0078	6	32.2	22	7	1.4	0.9	40	1.80	2.4	46	1
T34	2	0.25	32.2	5	0.0078	6	32.2	22	7	1.4	0.9	40	1.72	2.2	92	2
T35	2	0.25	32.2	5	0.0078	6	32.2	22	7	1.4	0.9	40	1.93	2.2	369	8

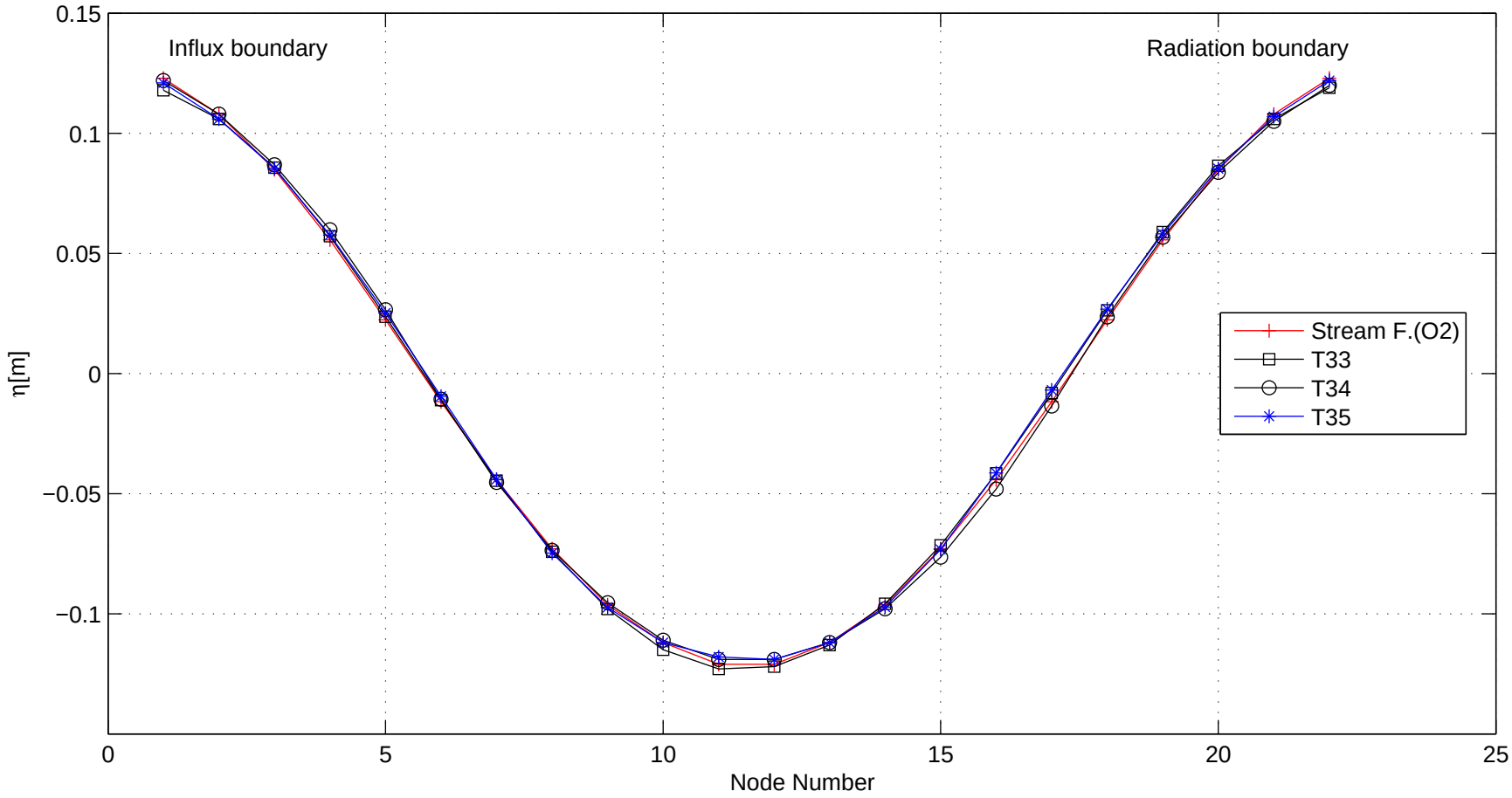

Figure 5.8. Variation of the free surface according to tests T33 to T35 (NMNI with second order stream function wave input and periodic boundary conditions)

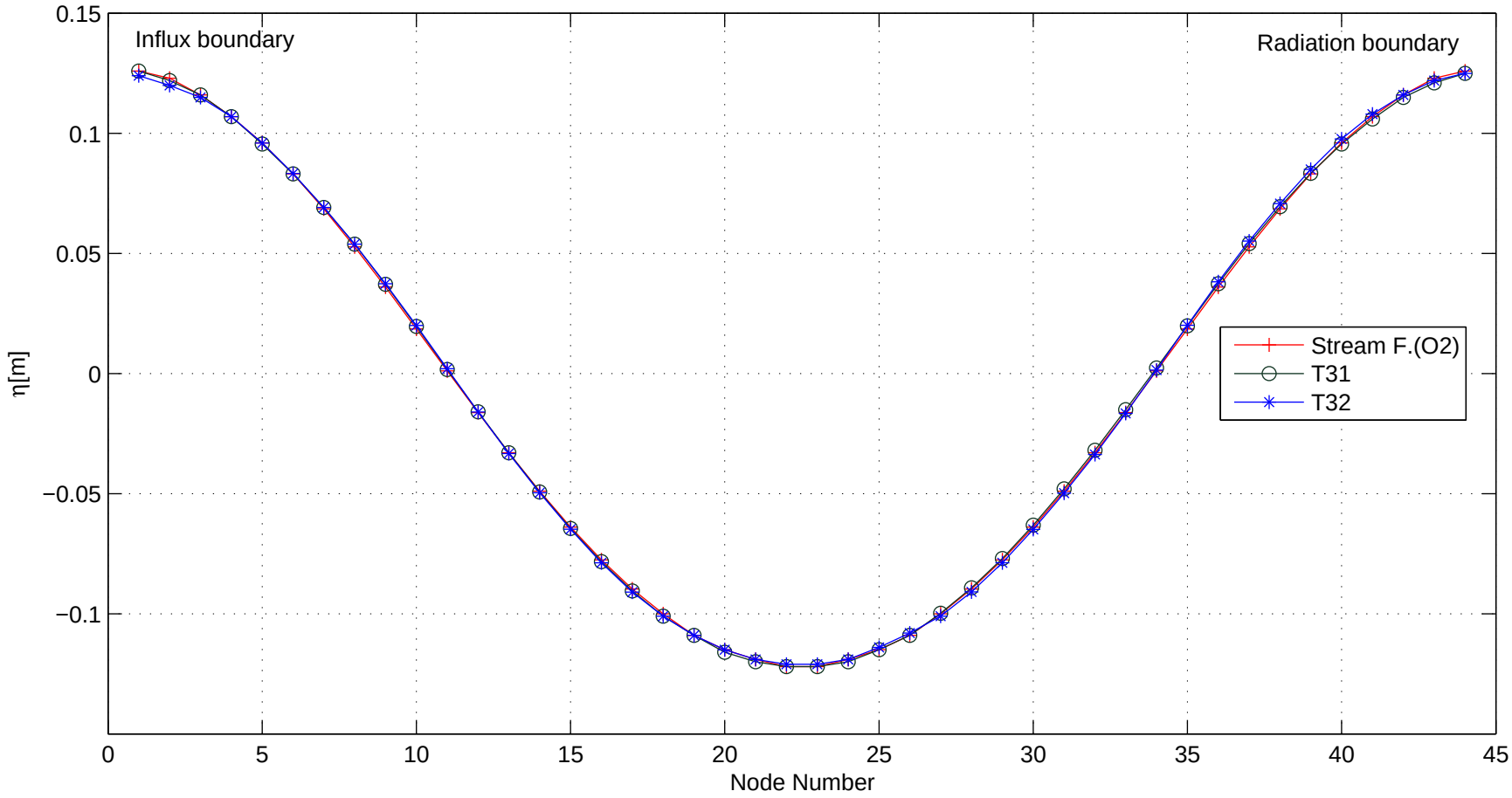

Figure 5.9. Variation of the free surface according to tests T31 to T32 (NMNI with second order stream function wave input and periodic boundary conditions)

Table 5.7. NMNI tests of a fourth order stream function wave

ID	Order	H[m]	L[m]	T[s]	H/L	d[m]	W[m]	nx	nz	dx	dz	c^2	ϵ%	ϵ_{rms}[mm]	R.T.[s]	nT
T36	4	0.25	21.1	5	0.0119	2	21.1	56	8	0.38	0.25	6	0.31	0.9	755	1
T37	4	0.25	21.1	5	0.0119	2	21.1	56	8	0.38	0.25	6	0.62	0.5	1544	2
T38	4	0.25	21.1	5	0.0119	2	21.1	56	8	0.38	0.25	6	0.62	0.8	3307	5

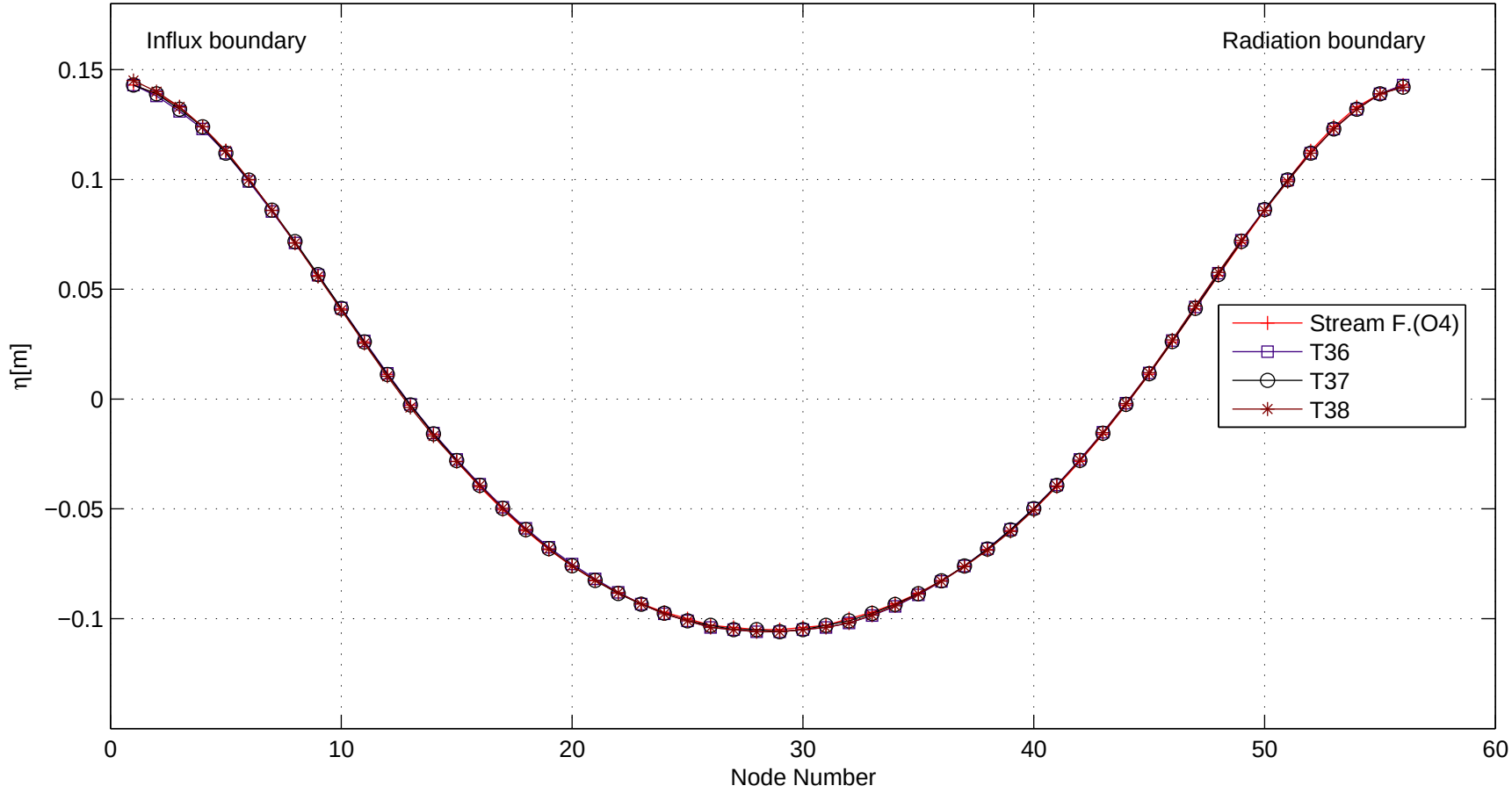

Figure 5.10. Variation of the free surface according to tests T36 to T38 of Table 5.7 (NMNI with fourth order stream function wave input and periodic boundary conditions)

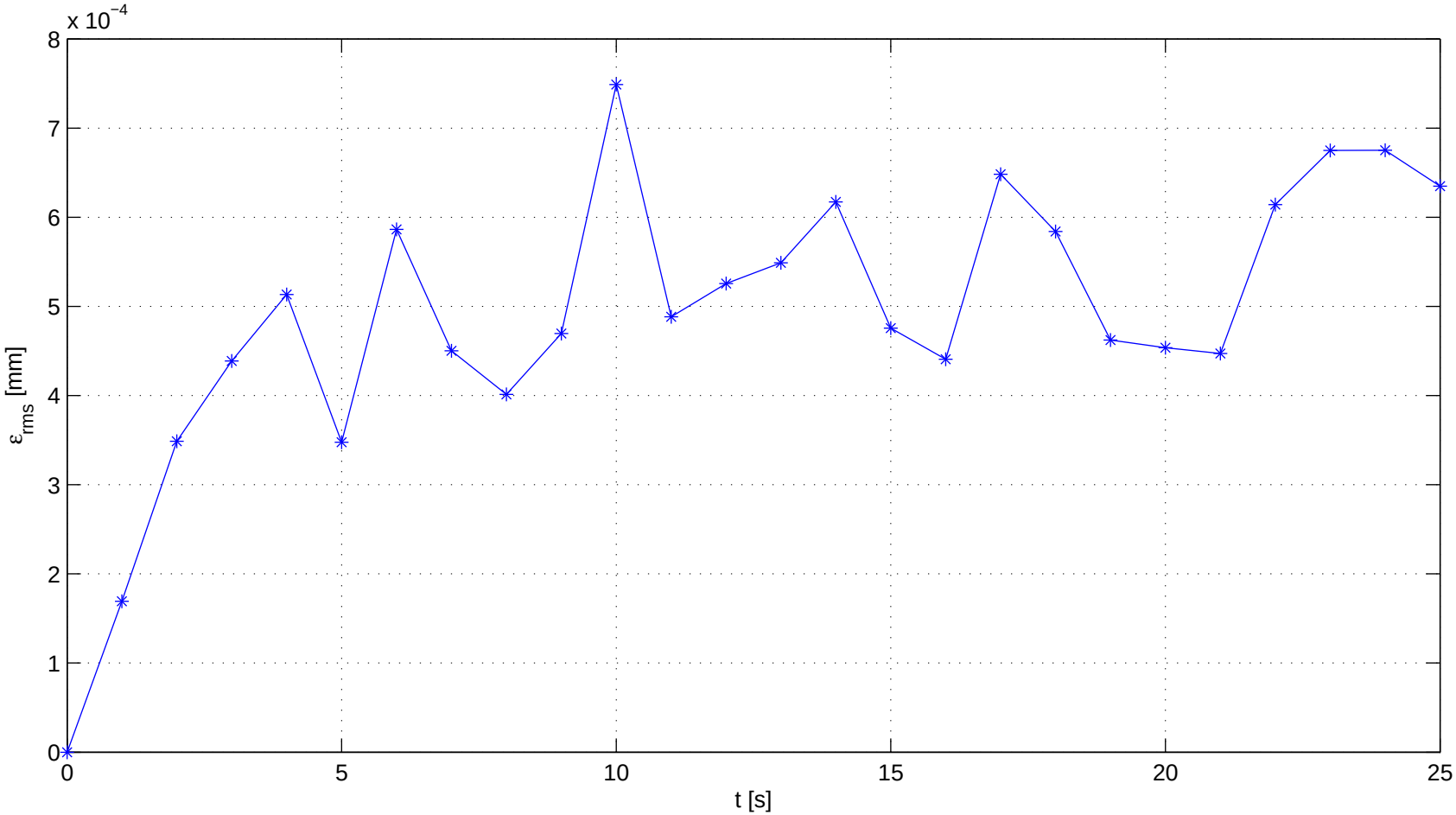

Figure 5.11. Variation of root mean square error corresponding to test T38 in time during 5 periods of real time computation

6. CONCLUSIONS AND RECOMMENDATIONS

This study shows that meshless MQ method can be applicable to the water wave propagation problem. The term applicability can be elaborated in terms of the efficiency and accuracy of the models developed in this study.

The MQ method here has proved itself to be an efficient method in the sense of the programming effort and the computation times. In general, two important tasks involved in numerical modeling, namely mesh generation and equation system construction requires much less effort than most of the counterpart modeling techniques. Even mesh generation for a problem with fixed boundaries, which is the linear problem in this study, the programming effort is almost negligible when compared to the time spent on the physics of the problem and time spent on complex mesh generation requiring techniques. Moreover, the nonlinear models that necessitate the inclusion of the surface deformation are handled easily. Therefore the efficiency of MQ method in terms of programming effort can be attributed to the fact that meshes are generated easily. Besides, computation times are also an important issue to talk about the efficiency of the models. Only considering tests using the waves with a period of 5 seconds, it can be said that relative error levels less than 1% of the wave height, are achieved on the average with 1 minute of simulation per period for the linear model and 15 minutes of simulation per period for the nonlinear models. Similarly, relative error levels around 2% of the wave height are achieved on the average with 5 seconds of simulation per period for the linear model and 40 seconds of simulation per period for the nonlinear models. Hence, according to these statistics, the method can be considered as efficient for the propagation of the waves investigated within the scope of this study.

Another important factor that determines the applicability of a method is the accuracy. The results are presented with the amplitude errors without mentioning the phase errors. As it was obvious from the free surfaces plotted at various instants the phase errors are negligible. The amplitude errors on the other hand are in acceptable levels and almost all of the maximum errors computed in the test are at the centers that

are close to the trough. This fact can be attributed to various reasons. One these is that the trough point is a critical point where the derivatives change sign so this may be a problem for the models making prediction using numerical approximations. Another reason is due to the nature of the methods using globally supported functions. Because pinning down smooth functions at its ends causes an increase in the errors at peak points. This can be observed by comparing the results of the NMLI with Sommerfeld radiation boundary condition and NMLI with periodic boundary condition. However in the case Sommerfeld radiation boundary condition is used, it has been observed that the solutions start to lack accuracy at the radiation boundary. In time this errors have grown and affected the solutions inside and eventually ended up with no solution.

At this point applicability of the model can be widened testing other known nonlinear models such as the Stokes waves of some order and the cnoidal waves. Also the wave steepness limits of the nonlinear model can be determined and if necessary improvements can be made in the model. The most important argument that needs fine tuning for steep waves is the shape parameter. Because it is taken as constant during the simulations, the optimum value of it is not adjusted to account for the center displacements in the vertical due to moving surface boundary. Given a wavelength, increasing the wave height increases the wave steepness, however this increases the difference between the vertical center spacings below the trough and crest. Hence, the high the wave is, the more the optimum ratio of consecutive center spacing in the horizontal to those in the vertical is affected. Therefore using variable shape parameter can be an improvement. Alternatively, sigma transformation can be used to make solutions at a uniform vertical distance. The sigma transformation may also be necessary if the wave is run over arbitrary profiles, instead of the horizontal bottom. On the other hand, augmenting the interpolation surface especially with the surfaces containing sines and cosines may improve the solutions.

REFERENCES

Airy, G.B., 1845, "Tides and Waves", *Encyclopedia Metropolitana*, Vol. 5.

Broeze, J., Van Daalen, E.F.G., 1992, "Radiation boundary conditions for the two-dimensional wave equation from a variational principle", *Mathematics of Computation*, Vol. 58(197), pp. 73-82.

Buhmann M.D., 2003, *Radial Basis Functions*, Cambridge University Press, Cambridge.

Burden, R.L., Faires, J.D., 1993, *Numerical Analysis*, 5th ed., PWS Publishing Company, Boston.

Dean, R.G., 1965, "Stream Function Representation of Nonlinear Ocean Waves", *Journal of Geophysical Research*, Vol. 70, No. 18, pp. 4561-4572.

Dean, R.G., Dalrymple, R.A., 1984,*Water Wave Mechanics for Engineers and Scientists*, Prentice-Hall Inc., Englewood Cliffs, New Jersey.

Dingemans, M.W., 1997, *Water Wave Propagation Over Uneven Bottoms:Part 1– Linear Wave Propagation*, World Scientific Publishing, Singapore.

Dingemans, M.W., 1997, *Water Wave Propagation Over Uneven Bottoms:Part 2– Nonlinear Wave Propagation*, World Scientific Publishing, Singapore.

Durran, D.R., 1998, *Numerical Methods for Wave Equations in Geophysical Fluid Dynamics*, Springer-Verlag, New York.

Engquist, B., Majda, A.,1977, "Absorbing Boundary Conditions for the Numerical Simulation of Waves",*Mathematics of Computation*, Vol. 31(139), pp. 629-651.

Fedoseyev, A.I., Friedman, M.J., Kansa, E.J., 2002,"Improved Multiquadric Method

for Elliptic Partial Differential Equations via PDE Collocation on the Boundary", *Computers and Mathematics with Applications* Vol. 43, pp. 439-455.

Fenton, J.D., 1988, "The Numerical Solution of Steady Water Wave Problems", *Computers& Structures*, Vol. 14, No. 3, pp. 357-368.

Fenton, J.D., Kennedy, A.B., 1996, "Fast methods for computing the shoaling of nonlinear waves", *Proceedings of the 25th International Conference on Coastal Engineering*, pp. 1130-1143.

Fornberg, B., Driscoll, T.A., Wright, G., Charles, R., 2002,"Observations on the Behavior of Radial Basis Function Approximations Near Boundaries", *Computers and Mathematics with Applications*, Vol. 43, pp. 473-490.

Franke, R. , 1982, "Scattered Data Interpolation: Test of Some Methods", *Mathematics of Computation*, Vol. 38, No. 157, pp. 181-200.

Golberg, M.A., Chen, C.S., Karur, S.R., 1996, "Improved multiquadric approximation for partial differential equations",*Engineering Analysis with Boundary Elements*, Vol.18, pp. 9-17.

Hardy, R.L., 1971, "Multiquadric equations of topography and other irregular surfaces", *Journal of Geophysical Research*, Vol. 76(26), pp. 1905-1915.

Higdon, R.L., 1986, "Absorbing boundary conditions for difference approximations", *Mathematics of Computation*, Vol.47(176), pp. 437-459.

Higdon, R.L., 1987, "Numerical absorbing boundary conditions for the wave equation", *Mathematics of Computation*, Vol.49(179), pp. 65-90.

Hon, Y.C., Kwok, Cheung, K.F., Mao, X.Z., Kansa E.J., 1999, "Multiquadric Solution for Shallow Water Equations", *Journal of Hydraulic Engineering*, Vol. 125, No. 5, pp. 524-533.

Isaacson, Mt. de St. Q., 1982, "Nonlinear-wave effects on fixed and floating bodies.", *Journal of Fluid Mechanics*, Vol. 120, pp. 267-281.

Israeli, M., Orszag, S.A., 1981, "Approximation of Radiation Boundary Conditions", *Journal of Computational Physics*, Vol. 41, pp.115-135.

Kansa, E.J., 1990a, "Multiquadrics - A Scattered Data Approximation Scheme with Applications to Computational Fluid Dynamics-I Surface Approximations and Partial Derivative Estimates", *Computers and Mathematics with Applications*, Vol. 19, No. 8/9, pp. 127-145.

Kansa, E.J., 1990b, "Multiquadrics- A Scattered Data Approximation Scheme with Applications to Computational Fluid Dynamics-II Solutions to Parabolic, Hyperbolic and Elliptic Partial Differential Equations", *Computers and Mathematics with Applications*, Vol. 19, No. 8/9, pp. 147-161.

Kennedy, A.B., Fenton, J.D., 1996, "A Fully Nonlinear 3D Method for the Computation of Wave Propagation", *Proceedings of the 25th International Conference on Coastal Engineering*, pp. 1102-1115.

Kennedy, A.B., Fenton, J.D., 1997, "A fully-nonlinear computational method for wave propagation over topography", *Coastal Engineering*, pp. 137-161.

Kowalik, Z., Murty, T.S., 1993, *Numerical Modeling of Ocean Dynamics*, World Scientific Publishing, Singapore.

Lin, W.-M., Newman, J.N., Yue, D.K., 1984, "Nonlinear forced motions of floating bodies", *Proceedings of the 15th Symposium on Naval Hydrodynamics, Hamburg*,pp.1-15.

Longuet-Higgins, M.S.,1953, "Mass transport in water waves",*Philosophical Transactions of the Royal Society of London. Series A*, Vol. 245, pp. 535-581, March.

Longuet-Higgins, M.S.,1960, "Mass-transport in the boundary layer at a free oscillating

surface",*Journal of Fluid Mechanics*, Vol. 8, pp. 293-306.

Longuet-Higgins, M.S., Cokelet, E.D., 1976, "The deformation of steep surface waves on water I. A numerical method of computation", *Proceedings of the Royal Society of London. A*, Vol. 350, pp. 1-26, July.

Madych, W.R., Nelson S.A., 1990, "Multivariate Interpolation and Conditionally Positive Definite Functions. II", *Mathematics of Computation*, Vol. 54, No. 189, pp. 211-230.

Mei, C.C., 1989, *The Applied Dynamics of Ocean Surface Waves*, World Scientific Publishing, Singapore.

Orlanski, I., 1976,"A simple boundary condition for unbounded hyperbolic flows", *Journal of Computational Physics*, Vol. 21, pp. 251-269.

Press, W.H., Teukolsky, S.A., Vetterling, W.T., Flannery, B.P., 1992, *Numerical Recipes in Fortran 77: The Art of Scientific Computing(Vol. 1 of Fortran Numerical Recipes)*, Cambridge University Press, Second Edition, New York.

Rienecker, M.M., Fenton, J.D., 1981, "A Fourier approximation method for steady water waves", *Journal of Fluid Mechanics*, Vol. 104, pp. 119-137.

Romate, J.E., 1989, *The Numerical Simulation of Nonlinear Gravity Waves in Three Dimensions Using a Higher Order Panel Method*, Ph.D. Dissertation, University of Twente, Netherlands.

Sommerfeld, A., 1949, *Partial differential equations in physics*, Academic Press, New York.

Stokes, G.G., 1847, "On the Theory of Oscillatory Waves", *Transactions of the Cambridge Philosophical Society*, Vol. 8.

Wendland, H., 1995, "Piecewise Polynomials, Positive Definite and Compactly Sup-

ported Radial Basis Functions of Minimal Degree", *Advances in Computational Mathematics*, Vol. 4, pp. 389-396.

Wu, Z., Hon, Y.C., 2003, "Convergence error estimate in solving free boundary diffusion problem by radial basis functions method", *Engineering Analysis with Boundary Elements*, Vol. 27, pp. 73-79.